Palaeogeography, Palaeoclimatology, Palaeoecology 535 (2019) 109346

Contents lists available at ScienceDirect

Palaeogeography, Palaeoclimatology, Palaeoecology

journal homepage: www.elsevier.com/locate/palaeo

Reconstructions of Antarctic topography since the Eocene–Oligocene boundary

Guy J.G. Paxman[a,*], Stewart S.R. Jamieson[a], Katharina Hochmuth[b,c], Karsten Gohl[b], Michael J. Bentley[a], German Leitchenkov[d,e], Fausto Ferraccioli[f]

[a] Department of Geography, Durham University, Durham, UK
[b] Alfred Wegener Institute Helmholtz-Center for Polar and Marine Sciences, Bremerhaven, Germany
[c] School of Geography, Geology and the Environment, University of Leicester, Leicester, UK
[d] Institute for Geology and Mineral Resources of the World Ocean, St. Petersburg, Russia
[e] Institute of Earth Sciences, St. Petersburg State University, St. Petersburg, Russia
[f] British Antarctic Survey, Cambridge, UK

A B S T R A C T

Accurate models of past Antarctic ice sheet behaviour require realistic reconstructions of the evolution of bedrock topography. However, other than a preliminary attempt to reconstruct Antarctic topography at the Eocene–Oligocene boundary, the long-term evolution of Antarctica's subglacial topography throughout its glacial history has not previously been quantified. Here, we derive new reconstructions of Antarctic topography for four key time slices in Antarctica's climate and glacial history: the Eocene–Oligocene boundary (ca. 34 Ma), the Oligocene–Miocene boundary (ca. 23 Ma), the mid-Miocene climate transition (ca. 14 Ma), and the mid-Pliocene warm period (ca. 3.5 Ma). To reconstruct past topography, we consider a series of processes including ice sheet loading, volcanism, thermal subsidence, horizontal plate motion, erosion, sedimentation and flexural isostatic adjustment, and validate our models where possible using onshore and offshore geological constraints. Our reconstructions show that the land area of Antarctica situated above sea level was ~25% larger at the Eocene–Oligocene boundary than at the present-day. Offshore sediment records and terrestrial constraints indicate that the incision of deep subglacial topographic troughs around the margin of East Antarctica occurred predominantly in the Oligocene and early Miocene, whereas in West Antarctica erosion and sedimentation rates accelerated after the mid-Miocene. Changes to the topography after the mid-Pliocene were comparatively minor. Our new palaeotopography reconstructions provide a critical boundary condition for models seeking to understand past behaviour of the Antarctic Ice Sheet, and have implications for estimating changes in global ice volume, temperature, and sea level across major Cenozoic climate transitions.

1. Introduction

Numerical ice sheet model simulations are widely used as a means of predicting the response of Earth's continental ice sheets to future climatic change, and in turn their contribution to global sea level rise (DeConto and Pollard, 2016; Golledge et al., 2015). These models are typically evaluated with recourse to their ability to reproduce past ice sheet behaviour during periods of warmer climate and ice sheet volume loss, which is constrained by geological and oceanographic data. A model that can successfully reproduce past ice sheet behaviour and extent can then, in principle, be used to make robust projections of future ice sheet response over timescales greater than the next few decades.

The Antarctic Ice Sheet (AIS) is the largest (containing ~58 m of sea level equivalent (Fretwell et al., 2013)) and most long-lived ice sheet on Earth. Although parts of the subglacial topography of Antarctica, such as the central highlands of East Antarctica, where the ice cover is frozen to the bed, have been little modified over the past 34 million years (Cox et al., 2010; Jamieson et al., 2010; Rose et al., 2013), other areas have been extensively modified by tectonics, erosion and isostatic adjustment (Jamieson et al., 2010; Krohne et al., 2016; Paxman et al., 2017; Wilson et al., 2012). Simulations of the past AIS have tended to rely on the modern bedrock topography, but in recent years it has become increasingly recognised that subglacial topography exerts a fundamental influence on the dynamics of the AIS (Austermann et al., 2015; Colleoni et al., 2018; Gasson et al., 2015; Wilson et al., 2013). It is therefore necessary to reconstruct past bedrock topography for particular time slices in order to accurately simulate AIS dynamics during those times in the past (Wilson et al., 2012). Using a more realistic subglacial topography has the potential to increase the robustness of ice sheet model results, and in turn engender greater confidence in projections of future ice sheet behaviour and sea level change.

* Corresponding author.
E-mail address: guy.j.paxman@durham.ac.uk (G.J.G. Paxman).

https://doi.org/10.1016/j.palaeo.2019.109346
Received 20 May 2019; Received in revised form 23 August 2019; Accepted 27 August 2019
Available online 28 August 2019

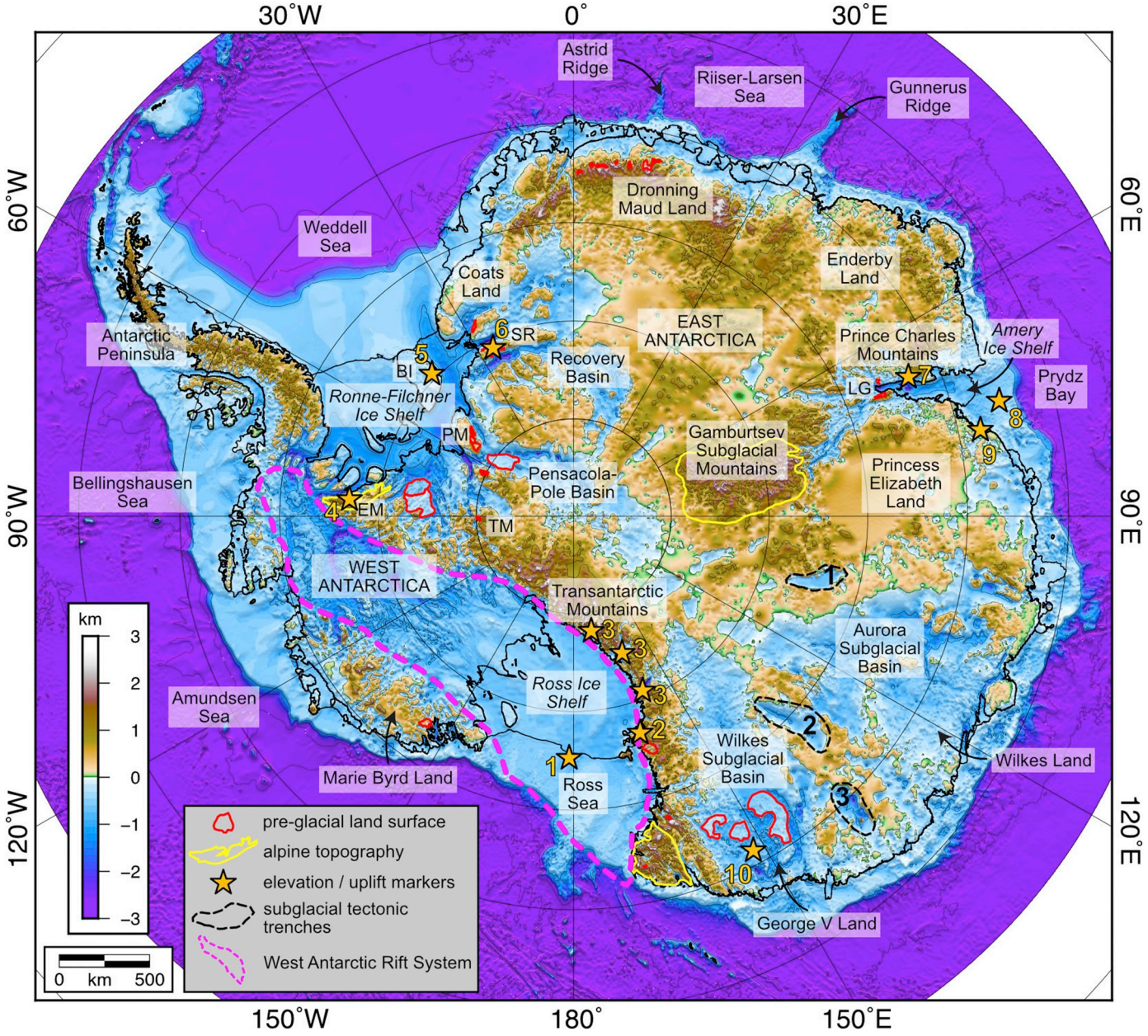

Fig. 1. Present-day bedrock topography of Antarctica. Major topographic features referred to throughout the text are labelled. Italicised labels denote major floating ice shelves. Topography is given as elevation above mean sea level, and is contoured at 1 km intervals. The smooth area in Princess Elizabeth Land is indicative of a data-poor region. Black lines demarcate the modern grounding line and ice calving front. Red polygons highlight pre-glacial land surfaces exposed above the ice sheet or preserved beneath the ice. Yellow polygons highlight regions characterised by alpine topography with a clear fluvial signature (Baroni et al., 2005; Rose et al., 2013; Sugden et al., 2017). Numbered orange stars mark the locations of palaeo-elevation/uplift markers (Section 5.1). Dashed black polygons mark subglacial trenches of inferred tectonic origin considered in our erosion model (Section 3.6.3); 1 = Lake Vostok; 2 = Adventure Subglacial Trench; 3 = Astrolabe Subglacial Trench. Dashed magenta outline marks the approximate onshore location of the West Antarctic Rift System (WARS) (Bingham et al., 2012; Jordan et al., 2010). Abbreviations: BI = Berkner Island; EM = Ellsworth Mountains; LG = Lambert Graben; PM = Pensacola Mountains; SR = Shackleton Range; TM = Thiel Mountains. (For interpretation of the references to colour in this figure legend, the reader is referred to the web version of this article.)

2. Background and aims

The aim of this study is to produce new reconstructions of Antarctic topography since glacial inception at the Eocene–Oligocene boundary (ca. 34 Ma). We aim to produce topographic reconstructions at the following time slices, which correspond to climatic transitions that are commonly the focus of ice sheet modelling studies:

- The Eocene–Oligocene boundary (ca. 34 Ma)
- The Oligocene–Miocene boundary (ca. 23 Ma)
- The mid-Miocene climate transition (ca. 14 Ma)
- The mid-Pliocene warm period (ca. 3.5 Ma)

We build upon previous work by Wilson and Luyendyk (2009) and Wilson et al. (2012) by beginning with the modern bedrock topography of Antarctica (Fig. 1) and reversing a series of geological processes that have acted to modify the topography since ca. 34 Ma. We incorporate a number of onshore and offshore datasets acquired or improved since these earlier reconstructions (see Section 3 and the supplementary material), and give consideration to the rate at which the landscape has evolved through time, rather than applying a simple linear interpolation between ca. 34 Ma and the present-day (Gasson et al., 2016). For

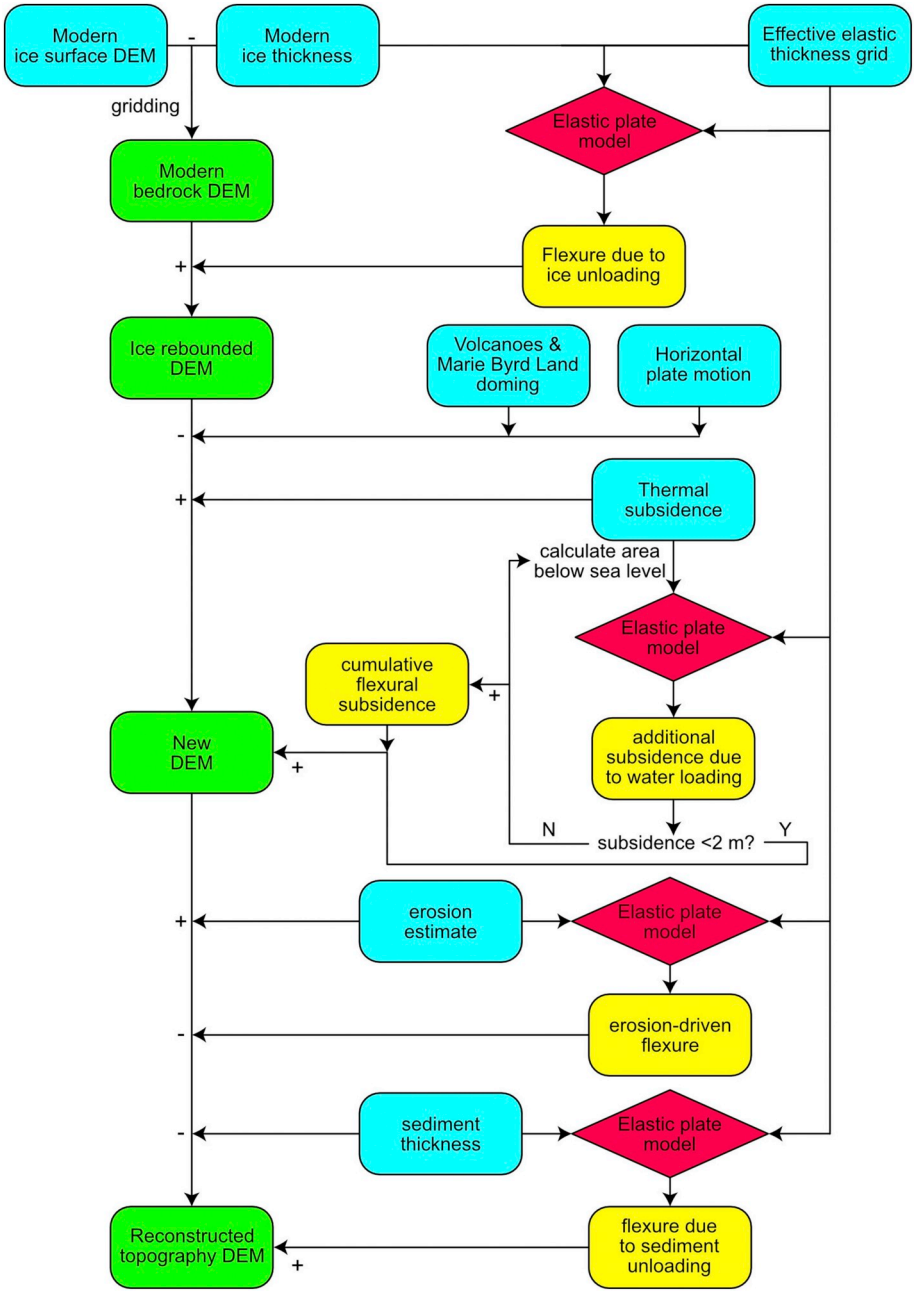

Fig. 2. Flow diagram of the topographic reconstruction process. Symbology: blue rectangles = input grids; red rhombs = elastic plate model used to compute flexural responses to load redistribution; yellow rectangles = outputs of flexural models; green rectangles = evolving bedrock topography DEMs. Note that the iteration scheme for calculating subsidence due to water loading is illustrated for the thermal subsidence step, but is also applied in each instance the elastic plate model is used. (For interpretation of the references to colour in this figure legend, the reader is referred to the web version of this article.)

each time slice, we produce a separate reconstruction of minimum and maximum topography, which provide end-member scenarios that encapsulate the cumulative uncertainties associated with each stage of the reconstruction process, and a median topography representing a 'middle-ground' between the two end-members (Section 3). We refrain from addressing the evolution of the oceanic realm (i.e. beyond the modern continental shelf edge), since this is the main focus of on-going work on the reconstruction of the palaeobathymetry of the Southern Ocean (Hochmuth et al., in prep.).

3. Reconstruction methods

In this section we describe the steps involved in our topographic reconstruction in the order in which they were performed (as summarised in Fig. 2). Several steps require the calculation of the isostatic response of the Antarctic lithosphere to surface load redistribution, which is computed using an elastic plate model that accounts for spatial variability in flexural rigidity (Chen et al., 2018) (for detail see the supplementary material). We also incorporate estimates of uncertainty associated with each step so as to construct minimum and maximum topographies. The values of each parameter assumed in our minimum, median and maximum reconstructions are shown in Supplementary Table 1. Each palaeotopography grid is produced at 5 km horizontal resolution and smoothed with a 10 km Gaussian filter to remove high frequency artefacts arising from the reconstruction process, without removing topographic features significantly larger than the grid resolution.

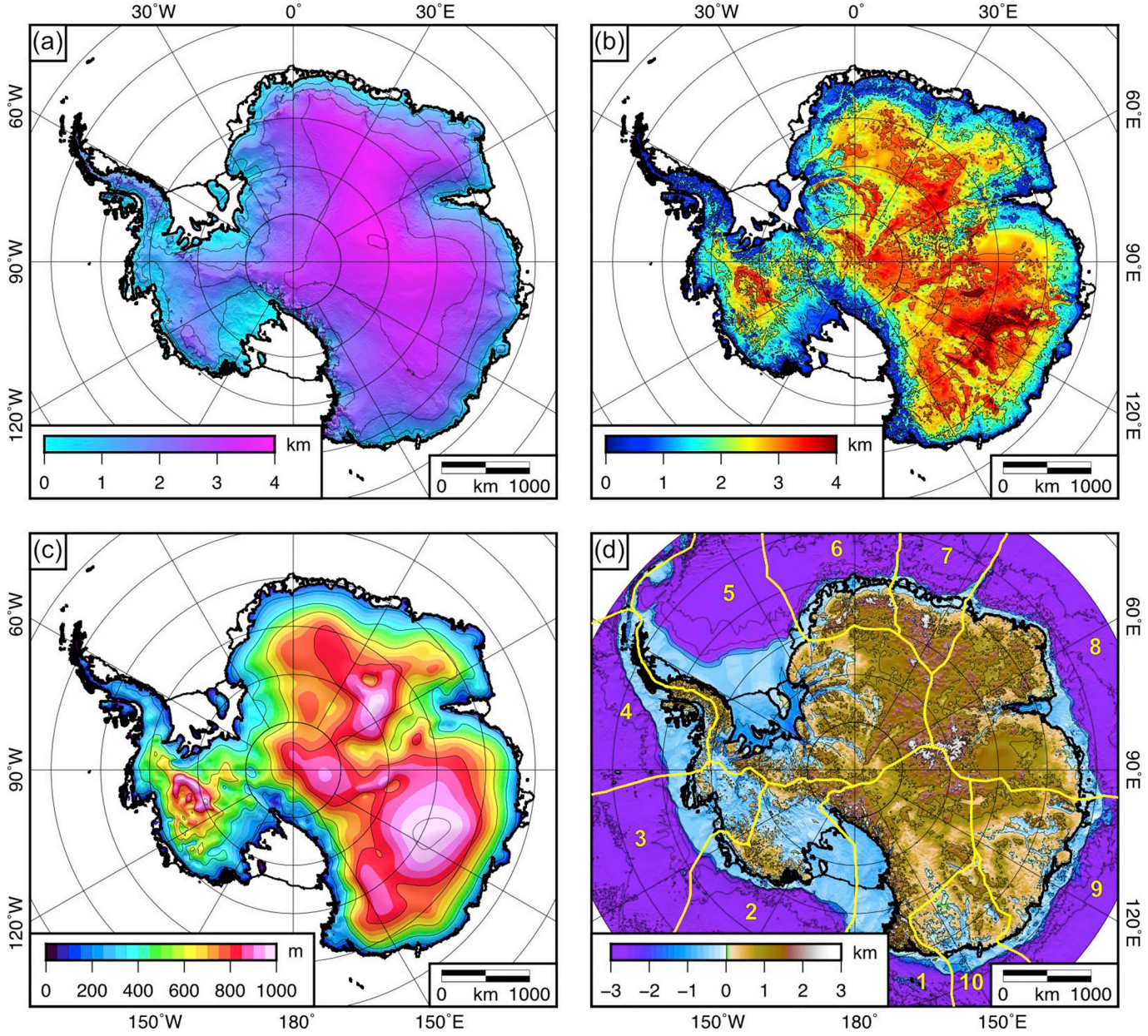

Fig. 3. Effect of ice loading on Antarctic topography. (a) Ice surface elevation (Slater et al., 2018). Elevations of grounded ice are shown relative to mean sea level, and contoured at 1 km intervals. (b) Ice thickness (the difference between ice surface (panel a) and bedrock (Fig. 1) elevation). The thickness of grounded ice (i.e. excluding floating ice shelves) is shown, and contoured at 1 km intervals. (c) Flexural isostatic rebound due to the removal of the present-day grounded ice load, contoured at 200 m intervals. (d) Bedrock topography after isostatic rebound due to the removal of the present-day ice load. Bedrock elevations are relative to mean sea level and contoured at 1 km intervals. Yellow lines show boundaries between sectors/catchments of the continent used to determine the balance between onshore erosion and offshore sedimentation. Each catchment is numbered for reference to Table 1. (For interpretation of the references to colour in this figure legend, the reader is referred to the web version of this article.)

3.1. Ice unloading

We determined the flexural response to the removal of the modern grounded ice sheet load (Fig. 3) using our updated ice thickness grid. We assumed ice and mantle densities of 920 and 3330 kg m^{-3} respectively and used a flexural model described in the supplementary material. We assumed a uniform 58 m sea level rise due to ice sheet removal, and computed the additional flexural response to water loading. Adjusting the topography for the removal of the ice sheet load modifies the geometry of the water load. Changes to the water load were iteratively calculated five times, whereupon the magnitude of the load change drops below 2 m (Jamieson et al., 2014; Wilson et al., 2012).

3.2. Volcanism

Cenozoic volcanoes have been documented in Victoria Land, Marie Byrd Land, and across the West Antarctic Rift System (WARS) (LeMasurier et al., 1990). Dating of volcanic edifices and associated deposits indicates that the majority of surviving volcanoes date from after the mid-Miocene (ca. 14 Ma) (LeMasurier and Landis, 1996; Rocchi et al., 2006; Shen et al., 2017; Stump et al., 1980). We therefore removed the volcanic edifices from our topographic reconstructions for ca. 34 Ma, ca. 23 Ma, and ca. 14 Ma, but retain all edifices in our ca. 3.5 Ma reconstruction. To remove the volcanoes from our topographies, we determined the approximate geometry of each edifice using a recent inventory of the distribution, height, and diameter of subglacial

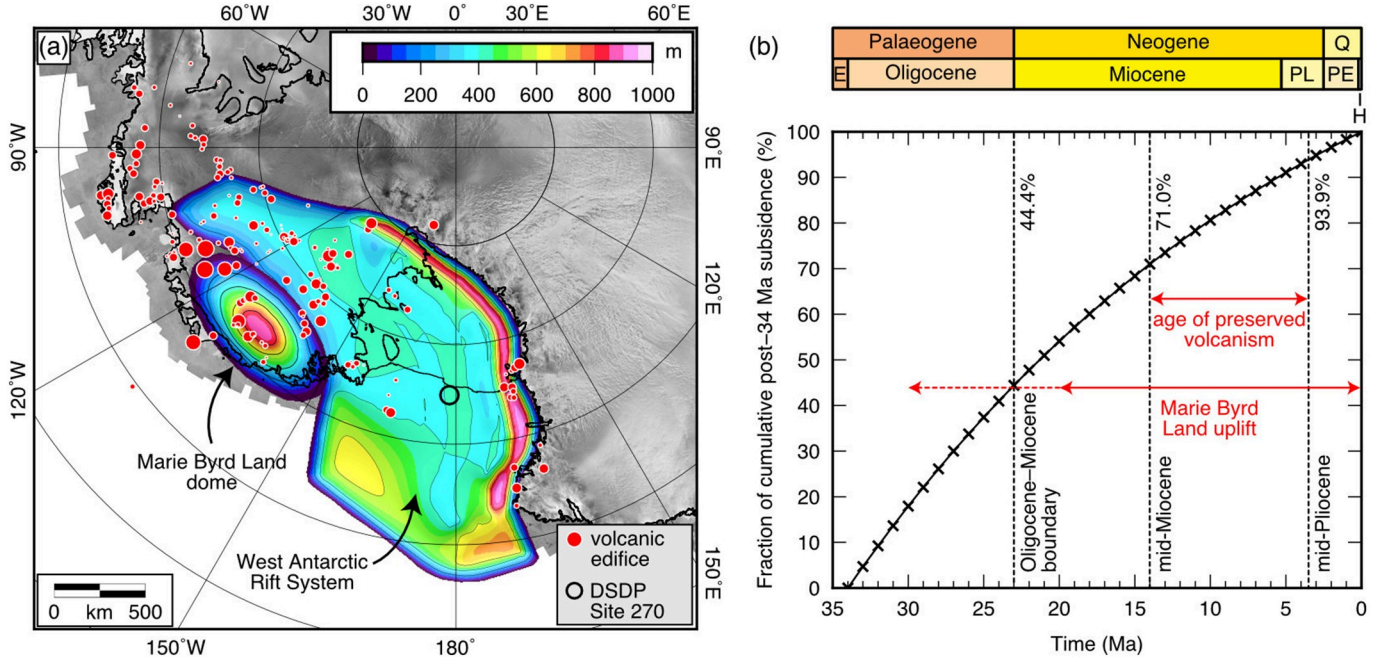

Fig. 4. Thermal subsidence, doming and volcanism in West Antarctica. (a) Magnitude of post-34 Ma thermal subsidence associated with the West Antarctic Rift System (Wilson et al., 2012; Wilson and Luyendyk, 2009) and domal uplift of Marie Byrd Land (Spiegel et al., 2016; Wilson et al., 2012). Filled red circles denote volcanic edifices across West Antarctica; circle size is proportional (4× true scale) to the basal diameter of the cone (van Wyk de Vries et al., 2018). Open black circle marks the location of Deep Sea Drilling Project (DSDP) Site 270 (Ford and Barrett, 1975). (b) Thermal subsidence history since 34 Ma based on a simple 1D cooling model (McKenzie, 1978). Cumulative subsidence is measured as a fraction of the total post-34 Ma subsidence; the magnitude of subsidence is spatially variable (see panel a). A simplified geological timescale is provided for reference. Abbreviations: E = Eocene; PL = Pliocene; PE = Pleistocene; H = Holocene; Q = Quaternary. The cumulative amount of subsidence from 34 Ma to each subsequent time slice used in this study (marked by vertical dashed lines) is noted as a percentage of the total subsidence. Also labelled are the approximate durations of Marie Byrd Land dome uplift (Spiegel et al., 2016) and the main episode of Miocene–Pliocene volcanism. (For interpretation of the references to colour in this figure legend, the reader is referred to the web version of this article.)

volcanic cones across West Antarctica (van Wyk de Vries et al., 2018) (Fig. 4), and then subtracted these cones from the topography. Since the wavelength of these features is typically shorter than the flexural length scale of the lithosphere (Watts, 2001), we do not account for flexural isostatic compensation of the edifices. Because the timing of volcanism is relatively well dated, we apply the same correction to each of our minimum, median and maximum reconstructions. We also adjusted for the adjacent uplift of the Marie Byrd Land dome (Section 3.7).

3.3. Horizontal plate motion

Although the relative motion between East and West Antarctica since 34 Ma is relatively minor, it is fairly well constrained by magnetic anomaly offsets of ~75 km in the Ross Sea (Cande et al., 2000; Davey et al., 2016). We follow Wilson and Luyendyk (2009) and Wilson et al. (2012) by applying a simple finite rotation to West Antarctica relative to East Antarctica of 1.14° about a fixed Euler pole (71.5°S, 35.8°W) (Supplementary Fig. 2). This horizontal plate motion largely occurred in the Oligocene (Cande et al., 2000), so we apply the rotation to our ca. 34 Ma reconstruction, but not to subsequent time slices, since any post-23 Ma rotations were likely small by comparison (Granot and Dyment, 2018). The rotation was applied to each of our minimum, median and maximum reconstructions.

3.4. Thermal subsidence

We restore the topography of West Antarctica for the effects of thermal subsidence in the WARS following previous studies (Wilson et al., 2012; Wilson and Luyendyk, 2006, 2009). The WARS is assumed to comprise five non-overlapping regions, each with a uniform stretching factor (β) and an instantaneous age of extension. These assumptions permit the use of a simple 1D cooling model to predict the amount of post-34 Ma thermal subsidence across the WARS (Fig. 4) (McKenzie, 1978; Wilson and Luyendyk, 2009). We then iteratively computed the flexural isostatic response to the flooding of the subsided area with water using our elastic plate model (see Section 3.1).

We also account for thermal subsidence of the East Antarctic passive margin due to residual cooling following Gondwana break-up. The breakup age of each sector of the Antarctic margin is well constrained from the age of the sea floor (Müller et al., 2016), although the initial timing of continental rifting is more difficult to assess. For simplicity, we assumed a uniform β value of 4 (a typical value for passive margins (Watts, 2001)) across the widths of the continent-ocean transitions around Antarctica (Gohl, 2008). Using the 1D cooling model (McKenzie, 1978), we calculated the amount of thermal subsidence to have occurred between 34 Ma and the present-day for each sector and then added this to the topography (Supplementary Fig. 3). The thermal subsidence grid was smoothed using an arbitrary 50 km Gaussian filter to approximate horizontal heat conduction. We applied a ± 10% uncertainty to our thermal subsidence models for the minimum and maximum reconstructions to encapsulate the range of realistic β values and rifting ages.

Application of the 1D cooling model also permits calculation of the temporal history of subsidence. The cumulative amount of thermal subsidence (as a fraction of the total subsidence) at any location is an exponential function of time and is independent of the stretching factor (Fig. 4). We therefore added the cumulative amount of subsidence from 34 Ma up to each time interval to the respective topographic reconstruction.

Extension within the WARS was a possible cause of rift-flank uplift of the Transantarctic Mountains (TAM) (ten Brink and Stern, 1992). While TAM uplift was originally believed to have occurred episodically throughout the Cretaceous and early Cenozoic (Fitzgerald and Stump, 1997), some recent thermochronological studies have suggested that

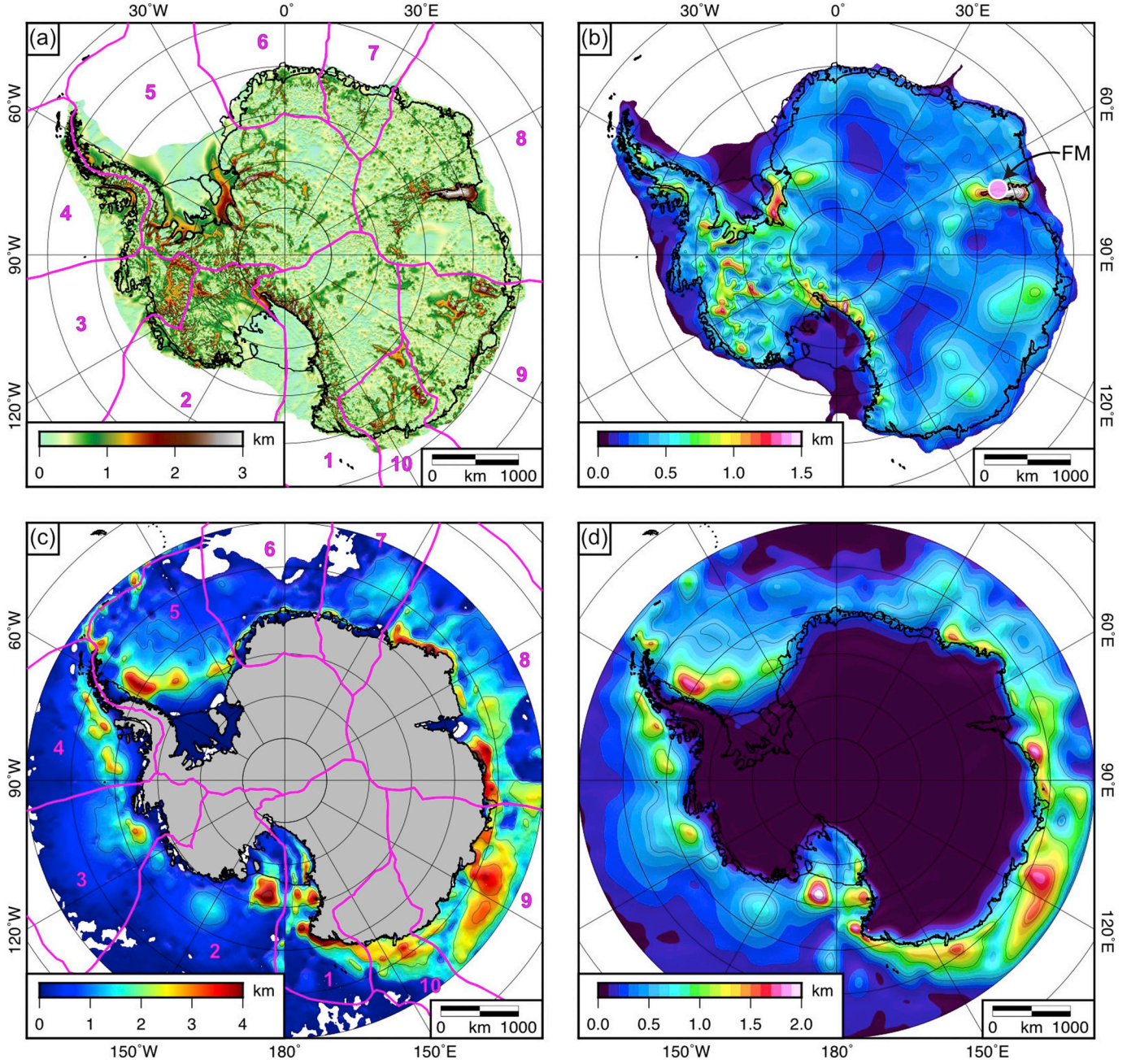

Fig. 5. Estimated post-34 Ma erosion and sediment thickness maps and associated isostatic responses. (a) Median eroded thickness scenario, with 1 km contour intervals. Magenta lines show boundaries between numbered sectors/catchments of the continent used to determine the balance between onshore erosion and offshore sedimentation. Each catchment is numbered for reference to Table 1. (b) Modelled flexural isostatic response to erosional unloading, contoured at 250 m intervals. Unloading of eroded material has driven isostatic uplift since 34 Ma; this component is subtracted from the modern-day topography to reconstruct past topographies. Coloured circle marks the magnitude of uplift of the Fisher Massif (FM; ~1500 m since 34 Ma) as constrained by geological data (Hambrey and McKelvey, 2000; White, 2013). (c) Post-34 Ma sediment thickness map for the Southern Ocean south of 60°S (Hochmuth et al., 2018). Sediment thicknesses are contoured at 1 km intervals. (d) Modelled flexural isostatic response to sediment loading, contoured at 500 m intervals. Loading of sediment has driven isostatic subsidence since 34 Ma; this component is added to the modern-day topography to reconstruct past topographies. (For interpretation of the references to colour in this figure legend, the reader is referred to the web version of this article.)

the TAM may have experienced rapid uplift and denudation immediately after glacial inception at ca. 34 Ma, resulting in the removal of the so-called 'Mesozoic Victoria Basin' (Lisker et al., 2014; Lisker and Läufer, 2013). Although this scenario remains subject to debate, it has implications for the regional palaeotopography at the Eocene–Oligocene boundary. However, the roles of thermal, erosional, tectonic and mantle-driven processes in driving TAM uplift remain poorly understood (Brenn et al., 2017; Paxman et al., 2019; Stern et al., 2005). We therefore make a simple adjustment to our minimum ca. 34 Ma palaeotopography by halving the elevation of the TAM following the adjustments for erosion and the associated flexural uplift (Section 3.6). This resulted in TAM palaeo-elevations comparable to those of the hinterland, in keeping with the end-member scenario of the possible presence of a pre-glacial sedimentary basin.

3.5. Offshore sedimentation

Sediment thicknesses on the continental shelf and in the deep sea

were derived from a recent compilation of reflection seismic data (Hochmuth et al., 2018; Sauermilch et al., 2019; Straume et al., 2019) (Fig. 5; for details see the supplementary material). The thickness (and mass) of offshore sediment can be used to (a) reconstruct the palaeobathymetry of the continental shelf and rise, and (b) constrain the mass of onshore erosion (Section 3.6). To produce each of our reconstructions, we removed all stratigraphic units younger than the time slice of interest, and subtracted or added the associated sediment thickness uncertainty (Supplementary Fig. 5) in our minimum and maximum topographies respectively.

3.5.1. Compaction model

We computed the flexural isostatic response to sediment loading using our elastic plate model. The density of shelf sediments varies with depth owing to mechanical compaction and reduction of porosity due to the overburden pressure. We used a simple compaction model to estimate the variation of sediment density with depth, whereby the decrease in sediment porosity (Φ) with increasing depth in the column (z) is given by an empirical exponential function (Sclater and Christie, 1980)

$$\phi(z) = \phi_0 \exp\left(-\frac{z}{\lambda}\right) \quad (1)$$

where Φ_0 is the initial porosity and λ is the compaction decay length scale. We then determined the depth-averaged effective density ($\overline{\rho_{eff}}$) of sediment around the Antarctic margin by removing the contribution from pore water, which is not restored to the continent.

$$\overline{\rho_{eff}}(x,y) = \rho_s(x,y)\left(1 - \frac{\lambda\phi_0}{z_{max}(x,y)}\left(1 - \exp\left(-\frac{z_{max}(x,y)}{\lambda}\right)\right)\right) \quad (2)$$

where ρ_s is the density of the sediment grains, and z_{max} is the total thickness of sediment being considered. For our median scenario, we assumed a grain density of 2600 kg m^{-3} for sediment on the continental shelf, and 2400 kg m^{-3} for deep-sea sediments (Sclater and Christie, 1980). We used values of 0.7 for the initial porosity and 1.0 km for the compaction decay length scale, based on empirical porosity-depth curves for Antarctic shelf sediments (Barker and Kennett, 1988; Escutia et al., 2011). We then used a realistic range of values for these parameters in our minimum and maximum reconstructions (Supplementary Table 1).

3.5.2. Terrigenous fraction

We estimated the fraction of offshore sediment that was derived from the continent as opposed to biogenic or pelagic material. We compared smear slide analysis from IODP/ODP/DSDP drill cores around the Antarctic margin representing the main sedimentary environments within the Southern Ocean (Barker and Kennett, 1988; Barker, 1999; Escutia et al., 2011). These data indicated that on the continental shelf, ~5% of material was biogenic, and the remaining ~95% was terrigenous in origin. In the deep ocean realm, ~70% of material from the Miocene to present is terrigenous, but this fraction increases to ~95% in the Oligocene. Although the spatial coverage of drill cores is sparse, and some localised variability is observed, this general trend is consistently observed. We therefore used the above average values, with ± 5% uncertainty bounds to encapsulate the majority of the spatial variability, around the entire margin. This is a more detailed terrigenous fraction model than that used in the earlier reconstructions by Wilson et al. (2012).

3.5.3. Catchment boundaries

When restoring sedimentary material to the continent and comparing the mass balance between erosion and sedimentation, it is important to consider the provenance of the offshore sediments. We therefore investigated whether offshore sediment around the Antarctic margin could be spatially sub-divided based on the geographic origin of the sediment. We sub-divided the sediment into ten sectors/catchments based on (a) boundaries mapped using geochemical provenance tracers such as $^{40}Ar/^{39}Ar$ ages and Nd isotopic compositions (e.g. Cook et al., 2013); (b) bathymetric 'highs' that form natural boundaries between separate basins on the continental shelf, such as Gunnerus Ridge and Astrid Ridge (Fig. 1) (Eagles et al., 2018); and (c) structural/basement highs observed in seismic data that may reflect geological boundaries, such as the Ross Sea Central High (Decesari et al., 2007).

We traced our assumed catchment boundaries over these previously documented features, and continued the boundaries inland based on observed ice surface velocity (Rignot et al., 2011) and bedrock drainage divides (Jamieson et al., 2014) (Figs. 2, 5). Our approach was to subdivide only if the boundary clearly met one of the above three criteria. The area of the sub-divided catchments therefore varies by up to one order of magnitude. We computed the minimum, median and maximum mass of post-34 Ma sediment for each catchment for comparison with our erosion estimate (Section 3.6).

3.6. Erosion restoration

3.6.1. Identification of pre-glacial landscapes

The morphology of the Antarctic landscape is a record of the surface processes that have acted upon it over geological timescales. To estimate the spatial distribution of glacial erosion across the continent, we identified landscapes or 'reference' relict surfaces that have been largely unmodified by large-scale glaciation, and have therefore experienced negligible erosion since ca. 34 Ma (Fig. 1). Such landscapes include undulating plateau surfaces exposed in highlands (Näslund, 2001; White, 2013) and observed beneath the ice around the Weddell Sea Embayment and within the Wilkes Subglacial Basin (Paxman et al., 2018; Rose et al., 2015), and alpine landscapes in the Gamburtsev Subglacial Mountains (GSM) (Paxman et al., 2016; Rose et al., 2013), Dronning Maud Land (DML) (Näslund, 2001), and the TAM (Sugden et al., 1999). In these regions, we assumed that the preserved mountain peaks have not experienced significant denudation or modification since ca. 34 Ma. Moreover, relatively unmodified fluvial valley systems are preserved in the northern TAM (Baroni et al., 2005; Sugden et al., 1995) and Ellsworth Mountains (Sugden et al., 2017), and the large-scale continental fluvial structure is still visible in the landscape today (Jamieson et al., 2014; Sugden and Jamieson, 2018).

3.6.2. Summit accordance

We consider glacial erosion to comprise two components: (1) selective linear erosion (valley/trough incision), and (2) uniform surface lowering via areal scour (Molnar and England, 1990; Sugden and John, 1976).

To estimate the spatial distribution of glacial valley incision, we assumed that pre-glacial landscape features identified across Antarctica once formed part of a contiguous surface prior to glacial incision. Since these pre-glacial land surfaces are sparsely distributed, we also identified local topographic 'highs' within a circular moving window (Champagnac et al., 2007). The diameter of the moving window was set to 30 km to capture the width of large subglacial troughs. We then interpolated a smooth continuous surface between all surfaces/summits, which are assumed to have not experienced significant erosion since AIS inception at 34 Ma. The resulting summit accordance surface (Supplementary Fig. 6) represents the restoration of eroded material to the topography without accounting for the associated isostatic response (Champagnac et al., 2007). The difference between the summit accordance surface and the bedrock topography represents our estimate of selective glacial incision (sometimes referred to as the 'geophysical relief' (Champagnac et al., 2007)).

In parts of Antarctica such as the GSM and TAM, a pre-existing fluvial landscape has been modified by alpine-style glaciation, and is now preserved beneath non-erosive ice (Sugden and Jamieson, 2018). By completely filling the valleys in these regions, we would likely

overestimate the amount of post-34 Ma erosion, and therefore produce an unrealistically smooth palaeolandscape. Mapping of glacial overdeepenings within the GSM indicates that glacial erosion accounts for—to first order—approximately 50% of the total volume of valley incision (Rose et al., 2013). We therefore decreased the predicted thickness of valley incision in these alpine landscapes by 50% in our erosion model. The result is a pre-glacial landscape that preserves the inherited fluvial valley network that was subsequently exploited by early ice sheets (Sugden and Jamieson, 2018; Sugden and John, 1976). We also adjusted the summit accordance surface and erosion estimate for deep subglacial trenches whose relief may, in part, be explained by tectonic subsidence as well as (or as opposed to) glacial erosion (see the supplementary material).

Accounting for valley incision alone will produce a minimum estimate of erosion, since it assumes that the peaks between the valleys have not been eroded. However, uniform surface lowering of the peaks since ca. 34 Ma is largely unconstrained by geomorphology. As a simple solution, we tuned the magnitude of uniform surface lowering to achieve as close a match as possible between the mass of eroded material and offshore sediment within each catchment for our minimum, median and maximum scenarios, while avoiding abrupt 'steps' in eroded thickness across catchment boundaries (Fig. 5; Supplementary Fig. 7; Table 1; Supplementary Table 2).

3.6.3. Eroded bedrock density and flexure

The subglacial geology of Antarctica, and therefore the density of the eroded bedrock, is almost entirely unconstrained. However, East Antarctica can be broadly considered to comprise a suite of rocks from higher-density Proterozoic and Archean metamorphic and magmatic basement (Boger, 2011; Ferraccioli et al., 2011; Goodge et al., 2017) to lower-density Palaeozoic sandstones (Barrett, 1991; Elliot et al., 2015). We therefore assumed a range of densities in East Antarctica from 2400 to 2800 $kg\,m^{-3}$ for our minimum and maximum reconstructions, and 2600 $kg\,m^{-3}$ as a realistic average. In West Antarctica, we assumed a range of 2200 to 2600 $kg\,m^{-3}$ to reflect the higher proportion of Mesozoic or younger sedimentary rocks (Studinger et al., 2001), with 2400 $kg\,m^{-3}$ as a realistic average. We then computed the flexural isostatic adjustment to erosional unloading using our elastic plate model. To correct the topography for the effects of erosion, we added the estimated post-34 Ma eroded thickness to the topography, and subtracted the associated flexural response.

3.6.4. Rates of erosion and sedimentation

To reconstruct topography at intermediate time slices, it was necessary to quantify the variation in erosion and sedimentation rates over time. We collated constraints on sedimentation rates from seismic reflection profiles and ocean sediment drill cores (Barker and Kennett, 1988; Escutia et al., 2011), assuming that sediment thickness depends on sedimentation rate alone, which in turn is a proxy for onshore erosion rates. We used these offshore sediment data together with onshore erosion rate constraints to estimate an erosion and sedimentation history for each of the ten catchments (Table 1), which we then used to restore the appropriate amount of eroded material/sediment between each time slice. In our reconstructions, we made the assumption that the catchment boundaries have remained constant over time, since the first-order topographic controls on Antarctic drainage patterns (e.g. the GSM and TAM) predate ice sheet inception (Rose et al., 2013), and the overall subglacial drainage pattern is continentally radial, and therefore drainage re-organisation is not expected to have occurred on a large scale (Sugden and Jamieson, 2018). We also assume that the offshore sediment boundaries have remained fixed over time, and that lateral transport of sediment by circumpolar currents is unlikely to have occurred in large volumes.

3.7. Dynamic topography

Long wavelength changes in bedrock elevation in Antarctica may, in part, be driven by vertical tractions exerted on the base of the lithosphere by the convecting mantle (i.e. dynamic topography). Changes in dynamic topography since the Eocene have been inferred in parts of Antarctica such as the Ross Sea, Wilkes Subglacial Basin and Marie Byrd Land (Austermann et al., 2015; LeMasurier and Landis, 1996). Since models of past mantle convection patterns are currently poorly constrained in space and time, we do not attempt to incorporate these changes here, with the exception of the post-34 Ma dynamic uplift of the Marie Byrd Land dome (Fig. 4).

We followed Wilson et al. (2012) by subtracting an elliptical Gaussian dome of 1000 km × 500 km diameter (Fig. 4) with a maximum amplitude of 1 km (LeMasurier and Landis, 1996) from our median ca. 34 Ma palaeotopography. We then corrected the more recent palaeotopographies assuming that uplift commenced at ca. 20 Ma and proceeded linearly to the present-day (Fig. 4), as indicated by recent thermochronology data (Spiegel et al., 2016). However, only four fission track ages were acquired from Marie Byrd Land, resulting in a large uncertainty in the ca. 20 Ma estimate (Spiegel et al., 2016). We allow for this uncertainty by changing the maximum amplitude of domal uplift to 2000 m and the beginning of uplift to ca. 30 Ma in our minimum reconstruction (Fig. 4) (LeMasurier and Landis, 1996; Rocchi et al., 2006), and foregoing this adjustment altogether in our maximum reconstruction.

We note that future robust models of post-34 Ma dynamic topography change across Antarctica can readily incorporated into our palaeotopographic reconstructions.

4. Results

The results of our reconstruction process are new topographies at four time slices between the Eocene–Oligocene boundary and mid-Pliocene warm period (Fig. 6). We find that the average bed elevation of Antarctica has decreased by ~200 m between ca. 34 Ma and the present-day (Table 2), and the interquartile range of bed elevations (a rough measure of topographic relief) has increased by ~200 m (Table 2). These changes are attributed largely to thermal subsidence, focussed erosion in deep subglacial troughs, and concomitant flexural uplift of the flanking regions. The increase in topographic relief is visible in the new palaeo-DEMs (Fig. 6), with an increasing fraction of the bed dropping below sea level (Supplementary Fig. 8). The area of land above sea level at ca. 34 Ma is 12.2×10^6 km^2, with ~6% of the bed situated below sea level, as opposed to 9.83×10^6 km^2 and ~19% respectively at the present-day (Table 2). These figures refer to the median topographies in each case; the minimum and maximum topographies are shown in Supplementary Figs. 9 and 10.

The most significant changes in elevation in East Antarctica occur within the Wilkes, Aurora, Recovery and Lambert basins, which were low-lying but predominately situated at 0–500 m above sea level prior to glacial inception (Fig. 6). Prior to thermal subsidence and erosion, a significant area of West Antarctica underlain by the WARS was also situated up to 500 m above sea level (Fig. 6). The Weddell Sea was a 500–1000 m deep embayment, the shallow extremities of which may have extended up to a few hundred km inland of the modern-day grounding line. The Ross Sea comprised a series of elongate horst and graben-like features, with topographic 'highs' such as the Central High situated at or just above sea level (Fig. 6). Our reconstruction retains the major highlands within East Antarctica, such as the GSM, TAM, and the escarpment in DML, with the GSM the highest feature at up to 2.5 km above sea level at ca. 34 Ma (Fig. 6). Because we only partially filled the valleys within the GSM, the pre-existing fluvial network can be seen in the ca. 34 Ma reconstruction. However, the through-cutting troughs that characterise the modern TAM have largely been filled in our reconstruction (Fig. 6). Our flexural models indicate that erosional

Table 1
Comparison between the mass of post-34 Ma offshore sediment and estimated onshore/shelf erosion for each catchment around Antarctica. Eroded masses and thicknesses listed refer to our median erosion scenario. Masses are given in Petatonnes (Pt; 10^{18} kg). Asterisks (*) mark the two sectors where the observed mass of sediment significantly exceeds erosion estimates. The mass of sediment in the Weddell Sea is likely to be a minimum estimate, since the thickness of sediment beneath the Ronne-Filchner Ice Shelf is entirely unconstrained. The erosion/sedimentation chronology is also provided for each catchment. The amount of erosion/sedimentation within the given time interval is given as a cumulative fraction of the total amount of change between 34 Ma and the present-day. Catchment averaged erosion rates are determined from the average eroded thickness and the fraction of erosion within each time interval.

Catchment	Computed mass of post-34 Ma offshore sediment (Pt)	Estimated mass of post-34 Ma eroded material (Pt)	Onshore area (10^6 km^2)	Average eroded thickness (m)	Cumulative fraction of post-Eocene change by 23 Ma	Cumulative fraction of post-Eocene change by 14 Ma	Cumulative fraction of post-Eocene change by 3.5 Ma	Average 34–23 Ma erosion rate (m/Myr)	Average 23–14 Ma erosion rate (m/Myr)	Average 14–0 Ma erosion rate (m/Myr)	References
1. Western Ross Sea	2.53	2.45	2.03	401	0.45	0.75	0.95	16.4	13.4	7.2	Hayes et al. (1975); Lindeque et al. (2016)
2. Eastern Ross Sea and Marie Byrd Land	2.14	1.90	1.05	548	0.30	0.50	0.95	14.9	12.2	19.6	Lindeque et al. (2016)
3. Amundsen Sea	1.09	1.06	0.72	656	0.30	0.50	0.90	17.9	14.6	23.4	Lindeque et al. (2016)
4. Bellingshausen Sea*	1.35	0.71	0.69	542	0.25	0.45	0.90	12.3	12.0	21.3	Lindeque et al. (2016)
5. Weddell Sea	3.88	4.47	3.98	469	0.25	0.40	0.92	10.7	7.8	20.1	Huang et al. (2014); Huang and Jokat (2016)
6. Dronning Maud Land margin	0.57	0.58	0.58	369	0.25	0.35	0.90	8.4	4.1	17.1	Barker and Kennett (1988)
7. Riiser-Larsen Sea	0.49	0.56	0.56	373	0.35	0.65	0.90	11.9	12.4	9.3	Castelino et al. (2016); Eagles et al. (2018)
8. Prydz Bay	3.25	3.31	2.81	450	0.40	0.80	0.92	16.4	20.0	6.4	Hambrey et al. (2007); Tochilin et al. (2012); Thomson et al. (2013); White (2013)
9. Wilkes Land margin*	3.48	2.20	1.66	507	0.35	0.70	0.92	16.1	19.7	10.9	Escutia et al. (2011); Tauxe et al. (2012)
10. George V Land coast	1.15	1.12	0.82	555	0.35	0.70	0.93	17.7	21.6	11.9	Escutia et al. (2011); Tauxe et al. (2012)
Total	19.93	18.36	14.89	481							

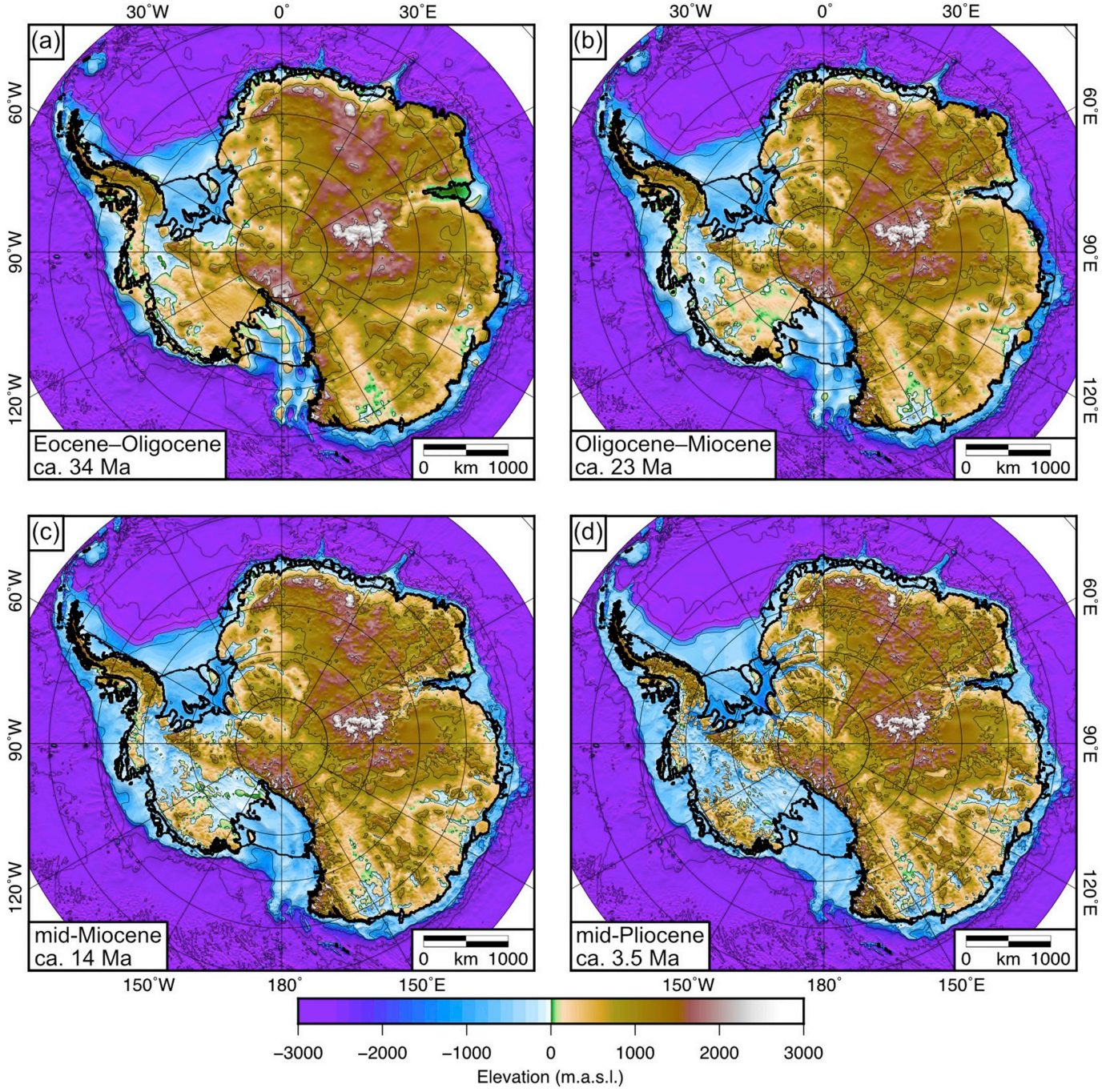

Fig. 6. Reconstructed topography maps for different time slices. For each time slice, the median topography is shown (minimum and maximum topographies are displayed in, and can be downloaded from, the supplementary material). (a) Antarctic topography at the Eocene–Oligocene boundary (ca. 34 Ma). (b) Antarctic topography at the Oligocene–Miocene boundary (ca. 23 Ma). (c) Antarctic topography at the mid-Miocene climate transition (ca. 14 Ma). (d) Antarctic topography at the mid-Pliocene (ca. 3.5 Ma). In each panel, elevations are given relative to present-day mean sea level, and contoured at 1 km intervals. Note that in each panel elevations are for fully isostatically relaxed ice-free conditions.

unloading has driven > 1 km of post-Eocene peak uplift in the southern TAM (Fig. 5), although the depth of some through-cutting troughs may be underestimated in the modern topography and the true amount of post-34 Ma uplift may have been greater (Paxman et al., 2019; Stern et al., 2005).

In seven of the ten catchments, we were able to achieve a close match (within ± 10%) between the mass of eroded material and mass of offshore sediment (Table 1) using our median erosion scenario (Section 3.6.2). By filling the deep subglacial troughs around the Weddell Sea Embayment, we estimate a mass of erosion that exceeds the mass of offshore sediment by ~20% (Table 1). This mismatch indicates that we may be missing a small but significant volume of sediment beneath the Ronne-Filchner Ice Shelf. Alternatively, a fraction of the sediment may have remained in onshore depocentres rather than deposited offshore. More significant mismatches occur for the Bellingshausen Sea and Wilkes Land sectors, where the eroded mass is ~50% less than the mass of offshore sediment (Table 1). However, there does not appear to be sufficient accommodation space onshore to account for this excess sediment.

One explanation may be that the mass of offshore sediment has been

Table 2
Statistical comparison of the different reconstructed and modern topographies in this study. Abbreviations: EOB = Eocene–Oligocene boundary; OMB = Oligocene–Miocene boundary; MMCT = mid-Miocene climate transition; MPWP = mid-Pliocene warm period.

Property	EOB (ca. 34 Ma)	OMB (ca. 23 Ma)	MMCT (ca. 14 Ma)	MPWP (ca. 3.5 Ma)	Modern (fully rebounded)	Modern (fully loaded)	Bedmap2 (fully loaded)
Mean bed elevation (m)	856	784	725	671	658	74.8	92.8
Median bed elevation (m)	866	792	737	701	693	74.4	84.0
Interquartile range of bed elevation (m)	859	920	958	1005	1024	872	858
Land area above sea level (10^6 km^2)	12.2	11.3	10.5	9.96	9.83	6.63	6.71
Proportion of bed below sea level (%)	5.94	8.91	14.0	18.0	19.1	45.3	44.6

overestimated due to the comparatively sparse coverage of seismic lines (Supplementary Fig. 4). Alternatively, since the geomorphology of Wilkes Land and the western Antarctic Peninsula does not provide a clear reference level of the palaeo-landscape (e.g. plateau surfaces), the summit accordance surface may be too low and the magnitude of erosion may have been underestimated. We speculate that these mismatches may also be attributed to redistribution of sedimentary material around the margin by contourite currents, a higher fraction of biogenic material, particularly near the Antarctic Peninsula (Barker, 1999), or a contribution from other sources including Large Igneous Provinces such as the Kerguelen Plateau. We note also that in Princess Elizabeth Land the modern-day bedrock topography is poorly constrained due to the lack of airborne radar observations included in Bedmap2 in this region and the landscape is artificially flat as it was derived from inversion of long wavelength satellite gravity data (Fretwell et al., 2013) (Fig. 1). Deeper subglacial topographic features in Princess Elizabeth Land have recently been identified (Jamieson et al., 2016), indicating that erosion is likely underestimated in this region.

Constraints on long-term changes in erosion and sedimentation rates from seismic sediment thickness, drill core, thermochronology and stratigraphic data (Table 1) show a broadly consistent temporal pattern around the East Antarctic margin. These records indicate that 65–75% of the erosion and sedimentation between DML and the western Ross Sea occurred prior to the mid-Miocene climate transition (ca. 14 Ma). By contrast, these proxies indicate that in West Antarctica (between the Weddell Sea and eastern Ross Sea), sedimentation rates were initially lower in the Oligocene and early Miocene, before accelerating after ca. 14 Ma (Lindeque et al., 2016) (Table 1). While spatial coverage of these records is patchy, and some local variability is observed, these broad patterns are consistently observed. Our reconstructions also confirm that the continental shelves have predominately grown outwards since ca. 34 Ma due to offshore sedimentation (Fig. 7) (Hochmuth and Gohl, 2019).

During the Oligocene, topographic change was largely dominated by subsidence in the West Antarctica and erosion around the East Antarctic margin (Fig. 7). By the mid-Miocene (ca. 14 Ma), East Antarctica's topography was beginning to more closely resemble that of the present-day. Overdeepenings had developed within the Wilkes and Aurora Subglacial Basins, and the Lambert Graben was > 1 km below sea level. Most of the WARS had subsided below sea level, other than a few isolated islands and the rising Marie Byrd Land dome (Fig. 6). Prior to ca. 14 Ma, catchment-averaged erosion rates were comparable in East and West Antarctica (Table 1). After ca. 14 Ma, average erosion rates accelerated to > 20 m/Myr in West Antarctica and around the Weddell Sea Embayment (Table 1), leading to the formation of deep subglacial troughs (Fig. 7). By contrast, erosion rates after ca. 14 Ma dropped by approximately 50% to ~10 m/Myr in East Antarctica, with landscapes such as the GSM remaining almost unmodified since ca. 14 Ma. Due to the relatively short interval of time, changes in elevation between 3.5 Ma and the present-day are relatively minor (Fig. 7).

One important caveat to note regarding the chronology of landscape change is that the rate of erosion through time is often inferred from the rate of offshore sedimentation. This is based on the assumption that long-term offshore sedimentation rates are a proxy for onshore erosion rates. However, the offshore depositional record may have been modified by hiatuses in sedimentation or erosional unconformities, which will violate this assumption. Moreover, it is likely that early glacial material was deposited on the continental shelf proximal to the coast, and subsequently transported and redeposited in deeper water by prograding wedges (Hochmuth and Gohl, 2019). As a result, the apparent 'depositional age' of the sediment may be significantly younger in places than the true age of erosion, which would lead to an unintentional bias towards more landscape change having occurred more recently than in actuality. While our model cannot constrain such an erosion pattern, we note the possibility that a greater proportion of the

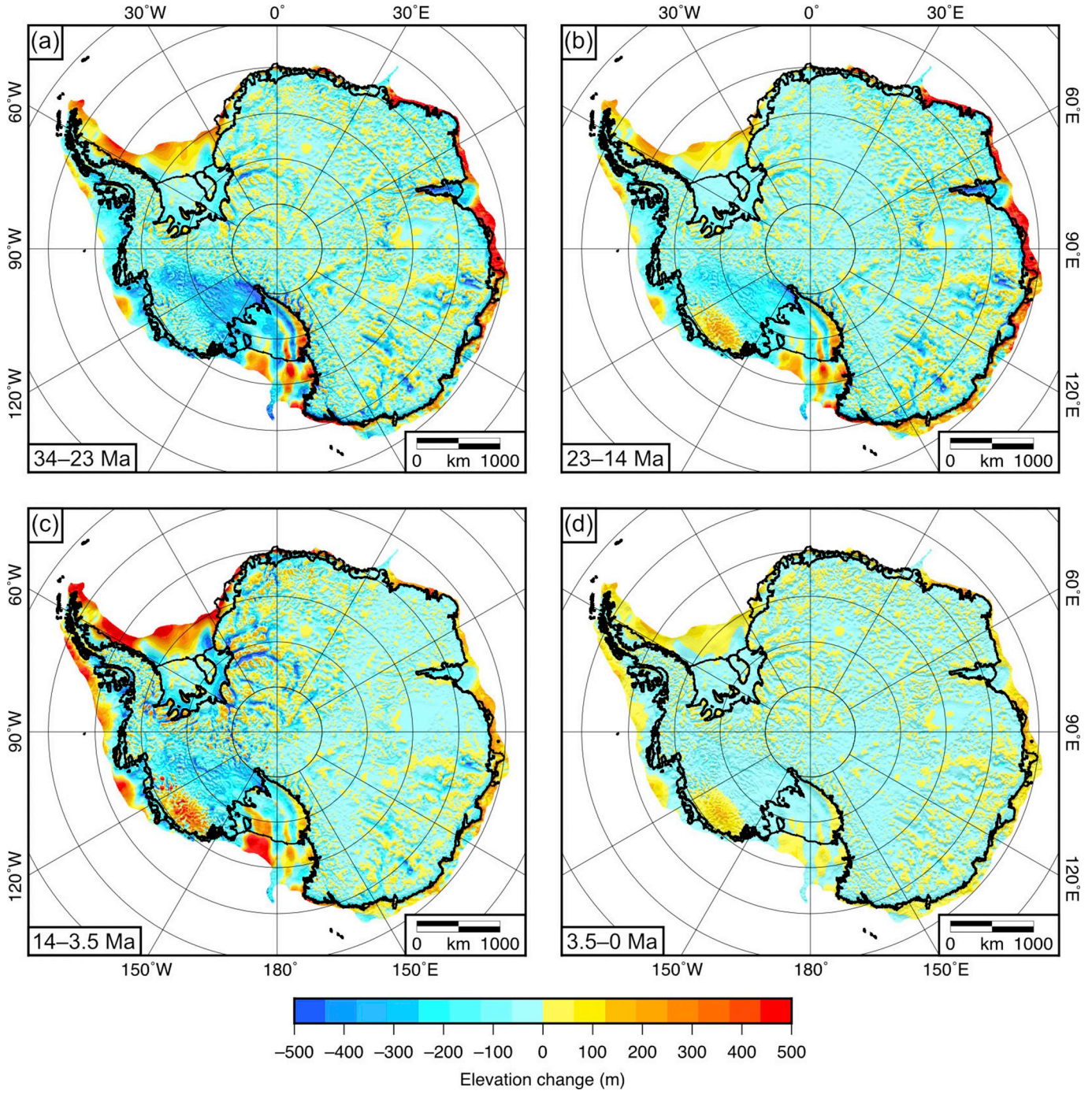

Fig. 7. Changes in bedrock elevation between time slices. In each panel, the difference in elevation (moving forward in time) between successive time slices is shown; warm colours denote uplift; cool colours denote subsidence. In each case, differences between median topographies are taken. (a) Change in elevation between 34 Ma and 23 Ma. (b) Change in elevation between 23 Ma and 14 Ma. (c) Change in elevation between 14 Ma and 3.5 Ma. (d) Change in elevation between 3.5 Ma and 0 Ma. During the first 20 million years, topographic change is largely dominated by subsidence in the West Antarctica and erosion around the East Antarctic margin. After ca. 14 Ma, erosion and sedimentation accelerate in West Antarctica and around the Weddell Sea Embayment, and decelerate in East Antarctica. (For interpretation of the references to colour in this figure legend, the reader is referred to the web version of this article.)

total amount of erosion may have occurred during the early stages of glaciation than is assumed in our reconstructions.

5. Discussion

5.1. Independent constraints on post-Eocene landscape evolution

Coring at DSDP Site 270 in the Ross Sea (Fig. 4) recovered a mature pre-Late Oligocene palaeosol several metres deep developed on a sedimentary breccia above basement gneiss at ~1000 m below sea level (Ford and Barrett, 1975). Our median reconstruction places this site at 80 m above sea level at the Eocene–Oligocene boundary (Fig. 6). The palaeosol is overlain by quartz sand and glauconitic greensand, which are dated at ca. 26 ± 1.5 Ma and interpreted as having been deposited in a near-shore or shallow marine environment (Barrett, 1975; De Santis et al., 1999; Kulhanek et al., 2019; Leckie and Webb, 1983). These sands are in turn overlain by an extensive sequence of glacio-marine sediments, indicative of a marine transgression and glacial

expansion (Kulhanek et al., 2019). Our median reconstruction indicates that this site subsided below sea level at ca. 28 Ma, which is in good agreement with the observed stratigraphy. In our minimum reconstruction (Supplementary Fig. 9), the site is already below sea level at ca. 34 Ma, whereas in our maximum reconstruction (Supplementary Fig. 10), the site does not subside below sea level until ca. 21 Ma. This highlights the conservative nature of our minimum and maximum reconstructions.

On the Fisher Massif in the Prince Charles Mountains (Fig. 5), post-Eocene fjordal sediments of the Pagodroma Group deposited close to sea level are exposed at up to 1.5 km above present-day sea level (Hambrey and McKelvey, 2000; White, 2013; Whitehead et al., 2003). Moreover, the age of Pagodroma Group deposits increases systematically with increasing elevation. Our erosion and flexure models suggest that up to 3 km of glacial excavation within the Lambert Graben has driven up to 1.4 km of flexural uplift along the graben flanks, which is within 100 m of the elevation of the oldest Pagodroma Group sediments. Combined with thermochronology data (Thomson et al., 2013; Tochilin et al., 2012), the observed apparent 'inverted stratigraphy' of the Pagodroma Group indicates a period of enhanced denudation in Oligocene and early Miocene times, and that flexural uplift has occurred throughout the Cenozoic and contemporaneous with fjordal sedimentation. We also note that matching this observational constraint is only possible if a relatively low (compared to other parts of East Antarctica) effective elastic thickness of 20 km is assumed for the East Antarctic Rift System (Ferraccioli et al., 2011).

Shallow marine sediments are also observed onshore at Marine Plain in the Vestfold Hills of East Antarctica (Fig. 1; Table 3). Sediments of the Pliocene Sørsdal Formation (ca. 4.5–4.0 Ma) were deposited in shallow/intertidal waters and are now situated 15–25 m above sea level (Pickard et al., 1988; Quilty et al., 2000). This site was situated within 10 m of sea level at 4 Ma in each of our reconstruction scenarios, and experienced ~20 m of uplift between 4 Ma and the present-day, which is in good agreement with the geological observations.

In the TAM, deep subglacial troughs are presently situated beneath large outlet glaciers such as Beardmore, Nimrod, Shackleton and Byrd. Palaeo-drainage and geomorphological evidence indicates that these deep troughs exploited pre-existing river valleys that were cut close to sea level (Huerta, 2007; Webb, 1994). In our ca. 34 Ma reconstruction, these valley systems were all situated between 0 and 500 m above sea level. Consequently, there were fewer drainage pathways that cut through the TAM, suggesting that more pre-glacial river systems may have drained into the Wilkes Subglacial Basin and towards George V Land than would be the case on the modern topography (Supplementary Fig. 11). The early East Antarctic Ice Sheet (EAIS) may have been unable to flow from the interior of East Antarctica through the TAM until sufficient overdeepening of through-cutting troughs allowed the EAIS to breach the TAM and drain into the Ross Sea. Further regional-scale geomorphological and thermochronological analysis may yield insights into the extent to which major valleys existed across the TAM prior to ca. 34 Ma.

The present-day elevation of a subaerially erupted lava flow in the Royal Society Range in the TAM (Fig. 1) indicates that there has been < 67 m of uplift at this site since 7.8 Ma (Sugden et al., 1999). Assuming a linear rate of erosion and uplift between the mid-Miocene and mid-Pliocene, our model predicts ~70 ± 20 m of uplift at this site since 7.8 Ma. Cinder-cone deposits in the Dry Valleys are also indicative of minimal surface uplift since the Pliocene (Wilch et al., 1993). Moreover, geomorphological evidence such as preserved ashfall deposits and rectilinear slopes add qualitative support to the scenario in which this part of the TAM has experienced minimal erosion and uplift since ca. 14 Ma (Marchant et al., 1993; Sugden et al., 1995).

Mountains on the margin of the Weddell Sea Embayment, such as the Shackleton Range and Ellsworth Mountains, have experienced up to 1 km of uplift since ca. 34 Ma due to flexure in response to erosional unloading within adjacent glacial troughs. The modelled pattern of uplift is supported by subaerial geomorphology, thermochronology, and cosmogenic nuclide dating evidence in the Shackleton Range (Krohne et al., 2016; Paxman et al., 2017; Sugden et al., 2014). In addition, thermochronological data from the Ellsworth Mountains

Table 3
Geological data used to constrain the landscape evolution of Antarctica. Each constraint is numbered according to its location (displayed in Fig. 1).

Location	Description and reference(s)	Constraint	Relevant time slice(s)
1. DSDP Site 270, Ross sea (178.5°W, 77.4°S)	Palaeosol overlain by early Oligocene quartz sands and glauconitic sands (Barrett, 1975; De Santis et al., 1999; Leckie and Webb, 1983).	Area was terrestrial at ca. 34 Ma and subsided beneath sea level at ca. 26 ± 1.5 Ma.	Eocene–Oligocene boundary; Oligocene–Miocene boundary
2. Royal Society Range and Dry Valleys, Transantarctic Mountains	Subaerial lava flow, in situ volcanic ash deposits and rectilinear slopes (Marchant et al., 1993; Sugden et al., 1999; Wilch et al., 1993)	< 67 m of surface uplift since 7.79 Ma; Relatively minimal erosion and uplift since ca. 14 Ma	Mid-Miocene; mid-Pliocene
3. Central Transantarctic Mountains	Inherited fluvial valleys systems and palaeo-drainage network (Huerta, 2007; Webb, 1994)	Valleys were situated above sea level and possibly cut close to base level	Eocene–Oligocene boundary
4. Ellsworth Mountains	Apatite fission track data from Mt. Vinson (Fitzgerald and Stump, 1991, 1992)	> 1.8 km of relief existed prior to the Cenozoic	Eocene–Oligocene boundary
5. Berkner Island (45.7°W, 79.5°S)	Sediments sampled at the base of the Berkner Island ice core (Mulvaney et al., 2007)	Aeolian sands indicative of transport above sea level but of unknown age	Unknown
6. Shackleton Range	Tilted bedrock plateau surfaces in Shackleton Range (Paxman et al., 2017)	Plateaux elevation and tilt constrain the magnitude and distribution of glacial erosion and flexure	Eocene–Oligocene boundary
7. Fisher Massif, Prince Charles Mountains (67.7°W, 72.3°S)	Pagodroma Group fjordal sediments deposited close to sea level currently situated up to 1.5 km above sea level (Hambrey et al., 2007; Hambrey and McKelvey, 2000; White, 2013)	Up to 1.5 km of flexural uplift since ca. 34 Ma	Eocene–Oligocene boundary and each subsequent time slice
8. ODP core site 188-1166A, Prydz Bay	Detrital thermochronology from offshore sediments of Cretaceous to Quaternary age (Cox et al., 2010; Thomson et al., 2013; Tochilin et al., 2012; van de Flierdt et al., 2008)	Acceleration of erosion rates in the early Oligocene and deceleration in the late Miocene. Up to 2.5 km of incision in the Lambert Graben since ca. 34 Ma.	Eocene–Oligocene boundary; Oligocene–Miocene boundary; mid-Miocene
9. Marine Plain, Vestfold Hills (78.0°E, 68.6°S)	Pliocene Sørsdal Formation comprising glaciomarine sediments deposited in shallow/intertidal waters now exposed 15–25 m above sea level (Pickard et al., 1988; Quilty et al., 2000)	Site was at or just below sea level at ca. 4.5–4 Ma, and was subsequently uplifted to its present-day elevation.	Mid-Pliocene
10. Wilkes Subglacial Basin	Subglacial geomorphology and offshore palynological records (Paxman et al., 2018; Sangiorgi et al., 2018)	Area was at or just above sea level, characterised by low-lying vegetated coastal plains	Eocene–Oligocene boundary; Oligocene–Miocene boundary

indicate that at least 1.8 km of relief was present prior to the glaciation (Fitzgerald and Stump, 1992); Mt. Vinson stands ~2 km above the floor of the Rutford trough in our ca. 34 Ma reconstruction.

Our erosion estimate shows relatively little incision across large areas within the interior of East Antarctica such as DML and the GSM (Fig. 5), supporting the findings of earlier ice sheet-erosion modelling studies (Jamieson et al., 2010). Geomorphological mapping of DML and the GSM reveals alpine glacial landscapes, which likely formed during the early stages of continental glaciation and have remained relatively unmodified for millions of years (Chang et al., 2015; Creyts et al., 2014; Rose et al., 2013). In these regions, our erosion estimates are indicative of long-term catchment-averaged erosion rates on the order of 10–20 m/Myr since at least 34 Ma, which are in good agreement with thermochronology data from detrital sediments in Prydz Bay (Fig. 1) (Cox et al., 2010; Tochilin et al., 2012; van de Flierdt et al., 2008).

An ice core from Berkner Island, an ice rise within the Ronne-Filchner Ice Shelf grounded on a shallow seabed plateau in the Weddell Sea, revealed that the ice is underlain by well-sorted, quartz-rich sands, which are interpreted as aeolian in origin but of unknown age (Mulvaney et al., 2007). The implication is that Berkner Island was situated above sea level when these sands were deposited. In our median reconstruction, the ice core location (Fig. 1) was situated 100–200 m above sea level (under ice-free conditions) since ca. 34 Ma. These aeolian sands may therefore have been transported at any time during an interval in which the core site was free of ice; without an age constraint for the sands, the topographic evolution of Berkner Island remains unclear.

5.2. Comparison with previous palaeotopography reconstructions

In our median Eocene–Oligocene boundary topography, much of West Antarctica is up to 500 m lower than the average topography of Wilson et al. (2012) (Supplementary Fig. 12). This is largely because we required a lower average thickness of eroded material to match constraints from updated offshore sediment records. We therefore do not produce such a substantial upland feature in West Antarctica. The total Antarctic land area above sea level in our median ca. 34 Ma reconstruction (12.2×10^6 km^2) is closer to the area in the minimum topography of Wilson et al. (2012) (12.7×10^6 km^2) than in their maximum topography (13.5×10^6 km^2). In East Antarctica, we find that differences in elevation are more subtle and shorter in wavelength (Supplementary Fig. 12). These differences likely reflect the improved modern bedrock DEM and offshore sediment thickness maps, both of which yield improved resolution in the reconstructed topographies.

Topographies for ca. 23 Ma and ca. 14 Ma were previously produced using a simple linear interpolation between the Wilson et al. (2012) topography and the present-day (Gasson et al., 2016). However, our model accounts for more complex temporal and spatial variability in erosion, sedimentation, thermal subsidence and isostasy. There are therefore differences between our ca. 23 Ma and ca. 14 Ma topographies and those of Gasson et al. (2016). Because thermal subsidence rates decay exponentially with time in our models as opposed to linearly as assumed by Gasson et al. (2016), West Antarctica is on average ~300 m lower at ca. 23 Ma in our scenario than in that of Gasson et al. (2016) (Supplementary Fig. 12). East Antarctic subglacial basins such as Wilkes and Aurora are ~200 m lower at ca. 23 Ma in our model than in that of Gasson et al. (2016) (Supplementary Fig. 12). By ca. 14 Ma, the differences are more subtle, with the largest differences located around the Weddell Sea, which may in part reflect the increased coverage of modern bedrock elevation data in this vicinity (Supplementary Fig. 1).

In a companion paper in this issue, Pollard and DeConto (2019) use a complementary model-based approach, explicitly integrating erosion and sedimentation processes forward in time. This approach produces maps of simulated past bedrock topography and 3D fields of modern sediment layers that can be compared directly with our results, providing insights into the strengths and uncertainties of both studies. Preliminary comparisons between the two studies are provided in the Supplementary Material of Pollard and DeConto (2019).

5.3. Implications for Antarctic glacial history

The evolution of Antarctica's subglacial topography raises a number of implications for the past behaviour of the AIS. The ca. 34 Ma topography has significantly less area below sea level and much shallower marine basins than the modern topography (Table 2; Supplementary Fig. 8). This implies that the early Antarctic ice sheets would have been less sensitive to climate and ocean forcing and less vulnerable to rapid and irreversible changes associated with marine ice sheet instability, since areas of reverse-sloping marine bed were less extensive and less steep (Fig. 6).

Our findings also have implications for the erosive history of the AIS. The incision of deep troughs transverse to the continental margin in East Antarctica during the Oligocene and early Miocene (Fig. 7) is indicative of a dynamic and erosive EAIS during this interval. After ca. 14 Ma, erosion/sedimentation rates appear to have decelerated markedly (Fig. 7), as is also implied by detrital thermochronology data from Prydz Bay (Tochilin et al., 2012). This change may have been climatically controlled, but may also reflect coastal subglacial troughs reaching a critical depth threshold, whereby the ice sheet was no longer able to avoid flotation, and the rate of erosion decreased. Such a scenario has been hypothesised for the Lambert Graben, which has been overdeepened to the extent that ice is unable to ground and advance onto the outer shelf without a significant increase in ice thickness, inhibiting significant further erosion (Taylor et al., 2004). By contrast, offshore sediment stratigraphic records indicate that West Antarctica witnessed an increase in erosion rates after the mid-Miocene (Lindeque et al., 2016) (Fig. 7). This may be indicative of the presence of more erosive, fluctuating ice sheets in West Antarctica after ca. 14 Ma.

The contrasting landscape and ice sheet histories of East and West Antarctica also have implications for marine ice sheet instability, whereby ice sheets grounded on inland-dipping bed below sea level can be subject to rapid and self-sustained retreat, a process thought to be particularly pertinent to the modern West Antarctic Ice Sheet (Joughin and Alley, 2011; Mercer, 1978; Vaughan et al., 2011). However, the implication of the landscape evolution scenario in this study is that prior to ca. 14 Ma, marine ice sheet ice sheet instability was most pertinent to the East Antarctic margin. After ca. 14 Ma, as West Antarctica had subsided below sea level and the bed was increasingly overdeepened, marine ice sheet instability would have become increasingly important in West Antarctica.

These new topographies also have important implications for modelling long-term changes in palaeoclimate, ice sheets, and sea level. Use of relevant palaeotopographies will be important when attempting quantify variations in Antarctica's ice volume and sea level contributions during past climate transitions at ca. 34, 23, 14, and 3.5 Ma, and thereby deconvolve ice volume and ocean temperature contributions from geochemical proxies such as benthic oxygen isotope records.

6. Conclusions

In this study, we have reconstructed Antarctic palaeotopography at four time intervals since the Eocene–Oligocene boundary (ca. 34 Ma). We conclude the following:

1. Our ca. 34 Ma topography contains a land area above sea level of 12.2×10^6 km^2, which is ~25% greater than at the present-day. The most significant changes in elevation in East Antarctica have occurred within the deep subglacial troughs close to the modern ice margin, some of which have been eroded by > 2 km. The low-lying Wilkes, Aurora and Recovery subglacial basins, which are thought to be particularly vulnerable to ice sheet retreat, were situated at 0–500 m above sea level at ca. 34 Ma. Much of the WARS was

situated up to 500 m above sea level, and has subsequently decreased in elevation due to thermal subsidence and glacial erosion.
2. Constraints from offshore sediment records, geomorphology, and geological datasets indicate that long-term catchment-averaged erosion rates are on the order 10–20 m/Myr. Erosion rates in East Antarctica decreased by ~50% after the mid-Miocene (ca. 14 Ma), whereas in West Antarctica, erosion rates approximately doubled after ca. 14 Ma. This implies that glaciers around the East Antarctic margin would have become vulnerable to marine ice sheet instability sooner than in West Antarctica.
3. Our new palaeotopographies provide an important boundary condition for models seeking to understand past behaviour of the Antarctic Ice Sheet, and the implications for changes in global ice volume, temperature, and sea level across major climate transitions of the Cenozoic.

Acknowledgements

GJGP is in receipt of a Natural Environment Research Council UK studentship NE/L002590/1 and was also supported by a Royal Astronomical Society grant. KH was funded by the German Research Foundation (DFG) grant GO274/15 and also acknowledges the tremendous help of J. Whittaker, I Sauermilch and the University of Tasmania Visiting Scholar scheme for additional funding during a research stay. FF acknowledges support from the British Antarctic Survey Geology and Geophysics team. We also wish to thank Mikhail Kaban for providing us with a grid of Antarctic effective elastic thickness. This research is a contribution to the Scientific Committee on Antarctic Research (SCAR) Past Antarctic Ice Sheet dynamics (PAIS) programme. We would like to acknowledge the support of numerous members of SCAR and PAIS and all contributors to the various ANTscape workshops on Antarctic palaeotopography and palaeobathymetry that were instrumental in the production of the topographies in this paper. We also thank Peter Barrett and Stuart Thomson for their constructive reviews, which greatly improved the final manuscript. The palaeotopography grids produced in this study are available online as supplementary material. Grids and figures were produced using the Generic Mapping Tools (GMT) software package version 5 (Wessel et al., 2013).

Appendix A. Supplementary data

Supplementary data to this article can be found online at https://doi.org/10.1016/j.palaeo.2019.109346.

References

Austermann, J., Pollard, D., Mitrovica, J.X., Moucha, R., Forte, A.M., DeConto, R.M., Rowley, D.B., Raymo, M.E., 2015. The impact of dynamic topography change on Antarctic ice sheet stability during the mid-Pliocene warm period. Geology 43, 927–930. https://doi.org/10.1130/G36988.1.

Barker, Peter F., 1999. Proceedings of the Ocean Drilling program, 178 initial reports. In: Barker, P.F., Camerlenghi, A., Acton, G.D. (Eds.), Proceedings of the Ocean Drilling Program, Initial Reports, Volume 178, Proceedings of the Ocean Drilling Program. Ocean Drilling Program, pp. 147–158. https://doi.org/10.2973/odp.proc.ir.178.1999.

Barker, P.E., Kennett, J.P. (Eds.), 1988. Proceedings of the Ocean Drilling Program, 113 Initial Reports, Proceedings of the Ocean Drilling Program. Ocean Drilling Program, College Station, Texas. https://doi.org/10.2973/odp.proc.ir.113.1988.

Baroni, C., Noti, V., Ciccacci, S., Righini, G., Salvatore, M.C., 2005. Fluvial origin of the valley system in northern Victoria Land (Antarctica) from quantitative geomorphic analysis. Geol. Soc. Am. Bull. 117, 212–228. https://doi.org/10.1130/B25529.1.

Barrett, P.J., 1975. Textural characteristics of Cenozoic preglacial and glacial sediments at Site 270, Ross Sea, Antarctica. Initial Reports Deep Sea Drill. Proj. Leg 28 (28), 757–767.

Barrett, P.J., 1991. The Devonian to Triassic Beacon Supergroup of the Transantarctic Mountains and correlatives in other parts of Antarctica. In: Tingey, R.J. (Ed.), The Geology of Antarctica. Oxford University Press, Oxford, UK, pp. 120–152.

Bingham, R.G., Ferraccioli, F., King, E.C., Larter, R.D., Pritchard, H.D., Smith, A.M., Vaughan, D.G., 2012. Inland thinning of West Antarctic Ice Sheet steered along subglacial rifts. Nature 487, 468–471. https://doi.org/10.1038/nature11292.

Boger, S.D., 2011. Antarctica — before and after Gondwana. Gondwana Res. 19, 335–371. https://doi.org/10.1016/j.gr.2010.09.003.

Brenn, G.R., Hansen, S.E., Park, Y., 2017. Variable thermal loading and flexural uplift along the Transantarctic Mountains, Antarctica. Geology 45, 463–466. https://doi.org/10.1130/G38784.1.

Cande, S.C., Stock, J.M., Müller, R.D., Ishihara, T., 2000. Cenozoic motion between East and West Antarctica. Nature 404, 145–150. https://doi.org/10.1038/35004501.

Castelino, J.A., Eagles, G., Jokat, W., 2016. Anomalous bathymetry and palaeobathymetric models of the Mozambique Basin and Riiser Larsen Sea. Earth and Planetary Science Letters 455, 25–37. https://doi.org/10.1016/j.epsl.2016.09.018.

Champagnac, J.D., Molnar, P., Anderson, R.S., Sue, C., Delacou, B., 2007. Quaternary erosion-induced isostatic rebound in the western Alps. Geology 35, 195–198. https://doi.org/10.1130/G23053A.1.

Chang, M., Jamieson, S.S.R., Bentley, M.J., Stokes, C.R., 2015. The surficial and subglacial geomorphology of western Dronning Maud Land, Antarctica. J. Maps 5647, 1–12. https://doi.org/10.1080/17445647.2015.1097289.

Chen, B., Haeger, C., Kaban, M.K., Petrunin, A.G., 2018. Variations of the effective elastic thickness reveal tectonic fragmentation of the Antarctic lithosphere. Tectonophysics 746, 412–424. https://doi.org/10.1016/j.tecto.2017.06.012.

Colleoni, F., De Santis, L., Montoli, E., Olivo, E., Sorlien, C.C., Bart, P.J., Gasson, E.G.W., Bergamasco, A., Sauli, C., Wardell, N., Prato, S., 2018. Past continental shelf evolution increased Antarctic ice sheet sensitivity to climatic conditions. Sci. Rep. 8, 11323. https://doi.org/10.1038/s41598-018-29718-7.

Cook, C.P., Van De Flierdt, T., Williams, T., Hemming, S.R., Iwai, M., Kobayashi, M., Jimenez-Espejo, F.J., Escutia, C., González, J.J., Khim, B.K., McKay, R.M., Passchier, S., Bohaty, S.M., Riesselman, C.R., Tauxe, L., Sugisaki, S., Galindo, A.L., Patterson, M.O., Sangiorgi, F., Pierce, E.L., Brinkhuis, H., Klaus, A., Fehr, A., Bendle, J.A.P., Bijl, P.K., Carr, S.A., Dunbar, R.B., Flores, J.A., Hayden, T.G., Katsuki, K., Kong, G.S., Nakai, M., Olney, M.P., Pekar, S.F., Pross, J., Röhl, U., Sakai, T., Shrivastava, P.K., Stickley, C.E., Tuo, S., Welsh, K., Yamane, M., 2013. Dynamic behaviour of the East Antarctic ice sheet during Pliocene warmth. Nat. Geosci. 6, 765–769. https://doi.org/10.1038/ngeo1889.

Cox, S.E., Thomson, S.N., Reiners, P.W., Hemming, S.R., van de Flierdt, T., 2010. Extremely low long-term erosion rates around the Gamburtsev Mountains in interior East Antarctica. Geophys. Res. Lett. 37. https://doi.org/10.1029/2010GL045106.

Creyts, T.T., Ferraccioli, F., Bell, R.E., Wolovick, M., Corr, H., Rose, K.C., Frearson, N., Damaske, D., Jordan, T., Braaten, D., Finn, C., 2014. Freezing of ridges and water networks preserves the Gamburtsev Subglacial Mountains for millions of years. Geophys. Res. Lett. 41, 8114–8122. https://doi.org/10.1002/2014GL061491.

Davey, F.J., Granot, R., Cande, S.C., Stock, J.M., Selvans, M., Ferraccioli, F., 2016. Synchronous oceanic spreading and continental rifting in West Antarctica. Geophys. Res. Lett. 43, 6162–6169. https://doi.org/10.1002/2016GL069087.

De Santis, L., Prato, S., Brancolini, G., Lovo, M., Torelli, L., 1999. The Eastern Ross Sea continental shelf during the Cenozoic: implications for the West Antarctic ice sheet development. Glob. Planet. Chang. 23, 173–196. https://doi.org/10.1016/S0921-8181(99)00056-9.

Decesari, R.C., Wilson, D.S., Luyendyk, B.P., Faulkner, M., 2007. Cretaceous and tertiary extension throughout the Ross Sea, Antarctica. In: Cooper, A.K. (Ed.), Antarctica: A Keystone in a Changing World – Online Proceedings of the 10th ISAES. U.S. Geol. Surv. Open File Rep.. https://doi.org/10.3133/of2007-1047.srp098. (2007–1047).

DeConto, R.M., Pollard, D., 2016. Contribution of Antarctica to past and future sea-level rise. Nature 531, 591–597. https://doi.org/10.1038/nature17145.

Eagles, G., Karlsson, N.B., Ruppel, A., Steinhage, D., Jokat, W., Läufer, A., 2018. Erosion at extended continental margins: insights from new aerogeophysical data in eastern Dronning Maud Land. Gondwana Res. 63, 105–116. https://doi.org/10.1016/j.gr.2018.05.011.

Elliot, D.H., Fanning, C.M., Hulett, S.R.W., 2015. Age provinces in the Antarctic craton: evidence from detrital zircons in Permian strata from the Beardmore Glacier region, Antarctica. Gondwana Res. 28, 152–164. https://doi.org/10.1016/j.gr.2014.03.013.

Escutia, C., Brinkhuis, H., Klaus, A., 2011. IODP expedition 318: from Greenhouse to icehouse at the Wilkes Land Antarctic Margin. Sci. Drill. 12, 15–23. https://doi.org/10.2204/iodp.sd.12.02.2011.

Ferraccioli, F., Finn, C.A., Jordan, T.A., Bell, R.E., Anderson, L.M., Damaske, D., 2011. East Antarctic rifting triggers uplift of the Gamburtsev Mountains. Nature 479, 388–392. https://doi.org/10.1038/nature10566.

Fitzgerald, P.G., Stump, E., 1991. Early cretaceous uplift in the Ellsworth Mountains of West Antarctica. Science 254, 92–94.

Fitzgerald, P.G., Stump, E., 1992. Early cretaceous uplift of the Southern Sentinel Range, Ellsworth Mountains, West Antarctica. In: Yoshida, Y., Kaminuma, K., Shiraishi, K. (Eds.), Recent Progress in Antarctic Earth Science - Proceedings of the Sixth International Symposium on Antarctic Earth Science. Terra Scientific Publishing Company (TERRAPUB), Tokyo, pp. 331–340.

Fitzgerald, P.G., Stump, E., 1997. Cretaceous and Cenozoic episodic denudation of the Transantarctic Mountains, Antarctica: new constraints from apatite fission track thermochronology in the Scott Glacier region. J. Geophys. Res. 102, 7747–7765.

Ford, A.B., Barrett, P.J., 1975. Basement rocks of the south-central Ross Sea, Site 270, DSDP Leg 28. Initial Reports Deep Sea Drill. Proj. Leg 28 (28), 861–868.

Fretwell, P., Pritchard, H.D., Vaughan, D.G., Bamber, J.L., Barrand, N.E., Bell, R., Bianchi, C., Bingham, R.G., Blankenship, D.D., Casassa, G., Catania, G., Callens, D., Conway, H., Cook, A.J., Corr, H.F.J., Damaske, D., Damm, V., Ferraccioli, F., Forsberg, R., Fujita, S., Gim, Y., Gogineni, P., Griggs, J.A., Hindmarsh, R.C.A., Holmlund, P., Holt, J.W., Jacobel, R.W., Jenkins, A., Jokat, W., Jordan, T., King, E.C., Kohler, J., Krabill, W., Riger-Kusk, M., Langley, K.A., Leitchenkov, G., Leuschen, C., Luyendyk, B.P., Matsuoka, K., Mouginot, J., Nitsche, F.O., Nogi, Y., Nost, O.A., Popov, S.V., Rignot, E., Rippin, D.M., Rivera, A., Roberts, J., Ross, N., Siegert, M.J., Smith, A.M., Steinhage, D., Studinger, M., Sun, B., Tinto, B.K., Welch, B.C., Wilson, D., Young, D.A., Xiangbin, C., Zirizzotti, A., 2013. Bedmap2: improved ice bed, surface and

thickness datasets for Antarctica. Cryosph. 7, 375–393. https://doi.org/10.5194/tc-7-375-2013.
Gasson, E., DeConto, R.M., Pollard, D., 2015. Antarctic bedrock topography uncertainty and ice sheet stability. Geophys. Res. Lett. 42, 5372–5377. https://doi.org/10.1002/2015GL064322.
Gasson, E., DeConto, R.M., Pollard, D., Levy, R.H., 2016. Dynamic Antarctic ice sheet during the early to mid-Miocene. Proc. Natl. Acad. Sci. 113, 3459–3464. https://doi.org/10.1073/pnas.1516130113.
Gohl, K., 2008. Antarctica's continent-ocean transitions: consequences for tectonic reconstructions. In: Cooper, A.K., Barrett, P.J., Stagg, H.M.J., Storey, B.C., Stump, E., Wise, W. (Eds.), Antarctica: A Keystone in a Changing World - Online Proceedings of the 10th ISAES. The National Academies Press, Washington, D.C., pp. 29–38. https://doi.org/10.3133/of2007-1047.kp04.
Golledge, N.R., Kowalewski, D.E., Naish, T.R., Levy, R.H., Fogwill, C.J., Gasson, E.G.W., 2015. The multi-millennial Antarctic commitment to future sea-level rise. Nature 526, 421–425. https://doi.org/10.1038/nature15706.
Goodge, J.W., Fanning, C.M., Fisher, C.M., Vervoort, J.D., 2017. Proterozoic crustal evolution of central East Antarctica: age and isotopic evidence from glacial igneous clasts, and links with Australia and Laurentia. Precambrian Res. 299, 151–176. https://doi.org/10.1016/j.precamres.2017.07.026.
Granot, R., Dyment, J., 2018. Late Cenozoic unification of East and West Antarctica. Nat. Commun. 9, 3189. https://doi.org/10.1038/s41467-018-05270-w.
Hambrey, M.J., McKelvey, B., 2000. Major Neogene fluctuations of the East Antarctic ice sheet: stratigraphic evidence from the Lambert Glacier region. Geology 28, 887–890. https://doi.org/10.1130/0091-7613(2000)28<887:MNFOTE>2.0.CO;2.
Hambrey, M.J., Glasser, N., McKelvey, B., Sugden, D., Fink, D., 2007. Cenozoic landscape evolution of an East Antarctic oasis (Radok Lake area, northern Prince Charles Mountains), and its implications for the glacial and climatic history of Antarctica. Quat. Sci. Rev. 26, 598–626. https://doi.org/10.1016/j.quascirev.2006.11.014.
Hayes, D.E., Frakes, L.A., the Shipboard Scientific Party, 1975. Initial Reports of the Deep Sea Drilling Project. Leg 28, 211–334.
Hochmuth, K., Gohl, K., 2019. Seaward growth of Antarctic continental shelves since establishment of a continent-wide ice sheet: patterns and mechanisms. Palaeogeogr. Palaeoclimatol. Palaeoecol. 520, 44–54. https://doi.org/10.1016/j.palaeo.2019.01.025.
Hochmuth, K., Gohl, K., Sauermilch, I., Whittaker, J.M., Leitchenkov, G., De Santis, L., Olivo, E., Uenzelmann-Neben, G., Davy, B.W., 2018. The Interlinked Cenozoic Evolution of Ocean Circulation Patterns and Antarctic Ice Sheets From Paleobathymetric Grids of the Southern Ocean. AGU Fall Meet. Abstr.
Hochmuth, K., Gohl, K., Sauermilch, I., Whittaker, J.M., Leitchenkov, G., DeSantis, L., Uenzelmann-Neben, G., Davy, B., 2019. A suite of paleobathymetric grids of the Cenozoic Southern Ocean - a key to understanding the interlinked evolution of ocean circulation patterns and Antarctic ice sheets. (in preparation).
Huerta, A.D., 2007. Byrd drainage system; evidence of a Mesozoic West Antarctic plateau. In: Cooper, A.K., Raymond, C.R. (Eds.), Antarctica: A Keystone in a Changing World – Online Proceedings of the 10th ISAES X: USGS Open-File Report 2007-1047. p. Extended Abstract 091, (5 p).
Huang, X., Gohl, K., Jokat, W., 2014. Variability in Cenozoic sedimentation and paleowater depths of the Weddell Sea basin related to pre-glacial and glacial conditions of Antarctica. Global and Planetary Change 118, 25–41. https://doi.org/10.1016/j.gloplacha.2014.03.010.
Huang, X., Jokat, W., 2016. Middle Miocene to present sediment transport and deposits in the Southeastern Weddell Sea, Antarctica. Global and Planetary Change 139, 211–225. https://doi.org/10.1016/j.gloplacha.2016.03.002.
Jamieson, S.S.R., Sugden, D.E., Hulton, N.R.J., 2010. The evolution of the subglacial landscape of Antarctica. Earth Planet. Sci. Lett. 293, 1–27. https://doi.org/10.1016/j.epsl.2010.02.012.
Jamieson, S.S.R., Stokes, C.R., Ross, N., Rippin, D.M., Bingham, R.G., Wilson, D.S., Margold, M., Bentley, M.J., 2014. The glacial geomorphology of the Antarctic ice sheet bed. Antarct. Sci. 26, 724–741. https://doi.org/10.1017/S0954102014000212.
Jamieson, S.S.R., Ross, N., Greenbaum, J.S., Young, D.A., Aitken, A.R.A., Roberts, J.L., Blankenship, D.D., Bo, S., Siegert, M.J., 2016. An extensive subglacial lake and canyon system in Princess Elizabeth Land, East Antarctica. Geology 44, 87–90. https://doi.org/10.1130/G37220.1.
Jordan, T.A., Ferraccioli, F., Vaughan, D.G., Holt, J.W., Corr, H., Blankenship, D.D., Diehl, T.M., 2010. Aerogravity evidence for major crustal thinning under the Pine Island Glacier region (West Antarctica). Bull. Geol. Soc. Am. 122, 714–726. https://doi.org/10.1130/B26417.1.
Joughin, I., Alley, R.B., 2011. Stability of the West Antarctic ice sheet in a warming world. Nat. Geosci. 4, 506–513. https://doi.org/10.1038/ngeo1194.
Krohne, N., Lisker, F., Kleinschmidt, G., Klugel, A., Laufer, A., Estrada, S., Spiegel, C., 2016. The Shackleton Range (East Antarctica): an alien block at the rim of Gondwana? Geol. Mag. 1–24. https://doi.org/10.1017/S0016756816001011.
Kulhanek, D.K., Levy, R.H., Clowes, C.D., Prebble, J.G., Rodelli, D., Jovane, L., Morgans, H.E.G., Kraus, C., Zwingmann, H., Griffith, E.M., Scher, H.D., McKay, R.M., Naish, T.R., 2019. Revised chronostratigraphy of DSDP Site 270 and late Oligocene to early Miocene paleoecology of the Ross Sea sector of Antarctica. Glob. Planet. Chang. 178, 46–64. https://doi.org/10.1016/j.gloplacha.2019.04.002.
Leckie, R.M., Webb, P.-N., 1983. Late Oligocene-early Miocene glacial record of the Ross Sea, Antarctica: evidence from DSDP Site 270. Geology 11, 578–582.
LeMasurier, W.E., Landis, C.A., 1996. Mantle-plume activity recorded by low-relief erosion surfaces in West Antarctica and New Zealand. Bull. Geol. Soc. Am. 108, 1450–1466. https://doi.org/10.1130/0016-7606(1996)108<1450:MPARBL>2.3.CO;2.
LeMasurier, W.E., Thomson, J.W., Baker, P.E., Kyle, P.R., Rowley, P.D., Smellie, J.L., Verwoerd, W.J. (Eds.), 1990. Volcanoes of the Antarctic Plate and Southern Oceans, Antarctic Research Series. American Geophysical Union, Washington, D. C. https://doi.org/10.1029/AR048.
Lindeque, A., Gohl, K., Wobbe, F., Uenzelmann-Neben, G., 2016. Preglacial to glacial sediment thickness grids for the Southern Pacific Margin of West Antarctica. Geochem. Geophys. Geosyst. 15, 1009–1020. https://doi.org/10.1002/2016GC006401.
Lisker, F., Läufer, A.L., 2013. The Mesozoic Victoria basin: vanished link between Antarctica and Australia. Geology 41, 1043–1046. https://doi.org/10.1130/G33409.1.
Lisker, F., Prenzel, J., Läufer, A.L., Spiegel, C., 2014. Recent thermochronological research in Northern Victoria Land, Antarctica. Polarforschung 84, 59–66.
Marchant, D.R., Denton, G.H., Sugden, D.E., Swisher, C.C., 1993. Miocene glacial stratigraphy and landscape evolution of the Western Asgard Range, Antarctica. Geogr. Ann. Ser. A. Phys. Geogr. 75, 303–330. https://doi.org/10.1080/04353676.1993.11880398.
McKenzie, D., 1978. Some remarks on development of sedimentary basins. Earth Planet. Sci. Lett. 40, 25–32. https://doi.org/10.1016/0012-821x(78)90071-7.
Mercer, J.H., 1978. West Antarctic ice sheet and CO_2 greenhouse effect: a threat of disaster. Nature 271, 321–325. https://doi.org/10.1073/pnas.0703993104.
Molnar, P., England, P., 1990. Late Cenozoic uplift of mountain ranges and global climate change: chicken or egg? Nature 346, 29–34. https://doi.org/10.1038/346029a0.
Müller, R.D., Seton, M., Zahirovic, S., Williams, S.E., Matthews, K.J., Wright, N.M., Shephard, G.E., Maloney, K.T., Barnett-Moore, N., Hosseinpour, M., Bower, D.J., Cannon, J., 2016. Ocean basin evolution and global-scale plate reorganization events since Pangea breakup. Annu. Rev. Earth Planet. Sci. 44, 107–138. https://doi.org/10.1146/annurev-earth-060115-012211.
Mulvaney, R., Alemany, O., Possenti, P., 2007. The Berkner Island (Antarctica) ice-core drilling project. Ann. Glaciol. 47, 115–124. https://doi.org/10.3189/172756407786857758.
Näslund, J.O., 2001. Landscape development in western and central Dronning Maud, East Antarctica. Antarct. Sci. 13, 302–311.
Paxman, G.J.G., Watts, A.B., Ferraccioli, F., Jordan, T.A., Bell, R.E., Jamieson, S.S.R., Finn, C.A., 2016. Erosion-driven uplift in the Gamburtsev Subglacial Mountains of East Antarctica. Earth Planet. Sci. Lett. 452, 1–14. https://doi.org/10.1016/j.epsl.2016.07.040.
Paxman, G.J.G., Jamieson, S.S.R., Ferraccioli, F., Bentley, M.J., Forsberg, R., Ross, N., Watts, A.B., Corr, H.F.J., Jordan, T.A., 2017. Uplift and tilting of the Shackleton Range in East Antarctica driven by glacial erosion and normal faulting. J. Geophys. Res. Solid Earth 122, 2390–2408. https://doi.org/10.1002/2016JB013841.
Paxman, G.J.G., Jamieson, S.S.R., Ferraccioli, F., Bentley, M.J., Ross, N., Armadillo, E., Gasson, E.G.W., Leitchenkov, G., DeConto, R.M., 2018. Bedrock erosion surfaces record former East Antarctic Ice Sheet extent. Geophys. Res. Lett. 45, 4114–4123. https://doi.org/10.1029/2018GL077268.
Paxman, G.J.G., Jamieson, S.S.R., Ferraccioli, F., Bentley, M.J., Ross, N., Watts, A.B., Leitchenkov, G., Armadillo, E., Young, D.A., 2019. The role of lithospheric flexure in the landscape evolution of the Wilkes Subglacial Basin and Transantarctic Mountains, East Antarctica. J. Geophys. Res. Earth Surf. 124, 812–829. https://doi.org/10.1029/2018JF004705.
Pickard, J., Adamson, D.A., Harwood, D.M., Miller, G.H., Quilty, P.G., Dell, R.K., 1988. Early Pliocene marine sediments, coastline, and climate of East Antarctica. Geology 16, 158–161. https://doi.org/10.1130/0091-7613(1988)016<0158:EPMSCA>2.3.CO;2.
Pollard, D., DeConto, R.M., 2019. Continuous simulations over the last 40 million years with a coupled Antarctic ice sheet-sediment model. Palaeogeography, Palaeoclimatology, Palaeoecology (this issue).
Quilty, P.G., Lirio, J.M., Jillett, D., 2000. Stratigraphy of the Pliocene sørsdal formation, marine plain, Vestfold hills, east Antarctica. Antarct. Sci. 12. https://doi.org/10.1017/S0954102000000262.
Rignot, E., Mouginot, J., Scheuchl, B., 2011. Ice flow of the Antarctic ice sheet. Science 333, 1427–1430. https://doi.org/10.1126/science.1208336.
Rocchi, S., LeMasurier, W.E., Di Vincenzo, G., 2006. Oligocene to Holocene erosion and glacial history in Marie Byrd Land, West Antarctica, inferred from exhumation of the Dorrel Rock intrusive complex and from volcano morphologies. Geol. Soc. Am. Bull. 118, 991–1005. https://doi.org/10.1130/B25675.1.
Rose, K.C., Ferraccioli, F., Jamieson, S.S.R., Bell, R.E., Corr, H.F.J., Creyts, T.T., Braaten, D., Jordan, T.A., Fretwell, P.T., Damaske, D., 2013. Early East Antarctic ice sheet growth recorded in the landscape of the Gamburtsev Subglacial Mountains. Earth Planet. Sci. Lett. 375, 1–12. https://doi.org/10.1016/j.epsl.2013.03.053.
Rose, K.C., Ross, N., Jordan, T.A., Bingham, R.G., Corr, H.F.J., Ferraccioli, F., Le Brocq, A.M., Rippin, D.M., Siegert, M.J., 2015. Ancient pre-glacial erosion surfaces preserved beneath the West Antarctic Ice Sheet. Earth Surf. Dyn. 3, 139–152. https://doi.org/10.5194/esurf-3-139-2015.
Sangiorgi, F., Bijl, P.K., Passchier, S., Salzmann, U., Schouten, S., McKay, R., Cody, R.D., Pross, J., Van De Flierdt, T., Bohaty, S.M., Levy, R., Williams, T., Escutia, C., Brinkhuis, H., 2018. Southern Ocean warming and Wilkes Land ice sheet retreat during the mid-Miocene. Nat. Commun. 9, 1–11. https://doi.org/10.1038/s41467-017-02609-7.
Sauermilch, I., Whittaker, J.M., Bijl, P.K., Totterdell, J.M., Jokat., W., 2019. Tectonic, Oceanographic, and Climatic Controls on the Cretaceous-Cenozoic Sedimentary Record of the Australian-Antarctic Basin. Journal of Geophysical Research: Solid Earth. https://doi.org/10.1029/2018JB016683.
Sclater, J.G., Christie, P.A.F., 1980. Continental stretching: an explanation of the Post-Mid-Cretaceous subsidence of the central North Sea Basin. J. Geophys. Res. Solid Earth 85, 3711–3739. https://doi.org/10.1029/JB085iB07p03711.
Shen, W., Wiens, D.A., Stern, T., Anandakrishnan, S., Aster, R.C., Dalziel, I., Hansen, S., Heeszel, D.S., Huerta, A., Nyblade, A., Wilson, T.J., Winberry, J.P., 2017. Seismic

evidence for lithospheric foundering beneath the southern Transantarctic Mountains, Antarctica. Geology 46, 1–4. https://doi.org/10.1130/G39555.1.
Slater, T., Shepherd, A., McMillan, M., Muir, A., Gilbert, L., Hogg, A.E., Konrad, H., Parrinello, T., 2018. A new digital elevation model of Antarctica derived from CryoSat-2 altimetry. Cryosph. 12, 1551–1562. https://doi.org/10.5194/tc-2017-223.
Spiegel, C., Lindow, J., Kamp, P.J.J., Meisel, O., Mukasa, S., Lisker, F., Kuhn, G., Gohl, K., 2016. Tectonomorphic evolution of Marie Byrd Land – implications for Cenozoic rifting activity and onset of West Antarctic glaciation. Glob. Planet. Chang. 145, 98–115. https://doi.org/10.1016/j.gloplacha.2016.08.013.
Stern, T.A., Baxter, A.K., Barrett, P.J., 2005. Isostatic rebound due to glacial erosion within the Transantarctic Mountains. Geology 33, 221–224. https://doi.org/10.1130/G21068.1.
Straume, E.O., Gaina, C., Medvedev, S., Hochmuth, K., Gohl, K., Whittaker, J.M., Abdul Fattah, R., Doornenbal, J.C., Hopper, J.R., 2019. GlobSed: Updated Total Sediment Thickness in the World's Oceans. Geochemistry, Geophys. Geosystems. https://doi.org/10.1029/2018GC008115.
Studinger, M., Bell, R.E., Blankenship, D.D., Finn, C.A., Arko, R.A., Morse, D.L., Joughin, I., 2001. Subglacial sediments: a regional geological template for ice flow in West Antarctica. Geophys. Res. Lett. 28, 3493–3496. https://doi.org/10.1029/2000GL011788.
Stump, E., Sheridan, M.F., Borg, S.G., Sutter, J.F., 1980. Early Miocene subglacial basalts, the East Antarctic ice sheet, and uplift of the transantarctic mountains. Science 207, 757–759. https://doi.org/10.1126/science.207.4432.757.
Sugden, D.E., Jamieson, S.S.R., 2018. The pre-glacial landscape of Antarctica. Scott. Geogr. J. 134, 203–223. https://doi.org/10.1080/14702541.2018.1535090.
Sugden, D.E., John, B.S., 1976. Glaciers and Landscape. Edward Arnold, London.
Sugden, D.E., Denton, G.H., Marchant, D.R., 1995. Landscape evolution of the dry valleys, transantarctic mountains: tectonic implications. J. Geophys. Res. 100, 9949–9967. https://doi.org/10.1029/94JB02875.
Sugden, D.E., Summerfield, M.A., Denton, G.H., Wilch, T.I., McIntosh, W.C., Marchant, D.R., Rutford, R.H., 1999. Landscape development in the royal society range, southern Victoria Land, Antarctica: stability since the mid-Miocene. Geomorphology 28, 181–200. https://doi.org/10.1016/S0169-555X(98)00108-1.
Sugden, D.E., Fogwill, C.J., Hein, A.S., Stuart, F.M., Kerr, A.R., Kubik, P.W., 2014. Emergence of the Shackleton Range from beneath the Antarctic Ice Sheet due to glacial erosion. Geomorphology 208, 190–199. https://doi.org/10.1016/j.geomorph.2013.12.004.
Sugden, D.E., Hein, A.S., Woodward, J., Marrero, S.M., Rodés, Á., Dunning, S.A., Stuart, F.M., Freeman, S.P.H.T., Winter, K., Westoby, M.J., 2017. The million-year evolution of the glacial trimline in the southernmost Ellsworth Mountains, Antarctica. Earth Planet. Sci. Lett. 469, 42–52. https://doi.org/10.1016/j.epsl.2017.04.006.
Tauxe, L., Stickley, C.E., Sugisaki, S., Bijl, P., Bijl, P.K., Bohaty, S.M., Brinkhuis, H., Escutia, C., Flores, J.A., Houben, A.J.P., Iwai, M., Jiménez-Espejo, F., McKay, R., Passchier, S., Pross, J., Riesselman, C.R., Rhl, U., Sangiorgi, F., Welsh, K., Klaus, A., Fehr, A., Bendle, J.A.P., Dunbar, R., Gonzlez, J., Hayden, T., Katsuki, K., Olney, M.P., Pekar, S.F., Shrivastava, P.K., van de Flierdt, T., Williams, T., Yamane, M., 2012. Chronostratigraphic framework for the IODP Expedition 318 cores from the Wilkes Land Margin: Constraints for paleoceanographic reconstruction. Paleoceanography 27, 1–19. https://doi.org/10.1029/2012PA002308.
Taylor, J., Siegert, M.J., Payne, A.J., Hambrey, M.J., O'Brien, P.E., Cooper, A.K., Leitchenkov, G., 2004. Topographic controls on post-Oligocene changes in ice-sheet dynamics, Prydz Bay region, East Antarctica. Geology 32, 197–200. https://doi.org/10.1130/G20275.1.
ten Brink, U.S., Stern, T.A., 1992. Rift flank uplifts and Hinterland Basins: comparison of the Transantarctic Mountains with the Great Escarpment of southern Africa. J. Geophys. Res. 97, 569–585. https://doi.org/10.1029/91JB02231.
Thomson, S.N., Reiners, P.W., Hemming, S.R., Gehrels, G.E., 2013. The contribution of glacial erosion to shaping the hidden landscape of East Antarctica. Nat. Geosci. 6, 203–207. https://doi.org/10.1038/ngeo1722.
Tochilin, C.J., Reiners, P.W., Thomson, S.N., Gehrels, G.E., Hemming, S.R., Pierce, E.L., 2012. Erosional history of the Prydz Bay sector of East Antarctica from detrital apatite and zircon geo- and thermochronology multidating. Geochem. Geophys. Geosyst. 13, 1–21. https://doi.org/10.1029/2012GC004364.
van de Flierdt, T., Hemming, S.R., Goldstein, S.L., Gehrels, G.E., Cox, S.E., 2008. Evidence against a young volcanic origin of the Gamburtsev Subglacial Mountains, Antarctica. Geophys. Res. Lett. 35, L21303. https://doi.org/10.1029/2008GL035564.
van Wyk de Vries, M., Bingham, R.G., Hein, A.S., 2018. A new volcanic province: an inventory of subglacial volcanoes in West Antarctica. Geol. Soc. Lond. Spec. Publ. 461, 231–248. https://doi.org/10.1144/SP461.7.
Vaughan, D.G., Barnes, D.K.A., Fretwell, P.T., Bingham, R.G., 2011. Potential seaways across West Antarctica. Geochem. Geophys. Geosyst. 12https://doi.org/10.1029/2011GC003688. (n/a-n/a).
Watts, A.B., 2001. Isostasy and Flexure of the Lithosphere. Cambridge University Press, Cambridge.
Webb, P.-N., 1994. Paleo-drainage systems of East Antarctica and sediment supply to West Antarctic rift system basins. Terra Antarct. 1, 457–461.
Wessel, P., Smith, W.H.F., Scharroo, R., Luis, J., Wobbe, F., 2013. Generic mapping tools: improved version released. EOS Trans. Am. Geophys. Union 94, 409–410. https://doi.org/10.1002/2013EO450001.
White, D.A., 2013. Cenozoic landscape and ice drainage evolution in the Lambert Glacier-Amery Ice Shelf system. Geol. Soc. Lond. Spec. Publ. 381, 151–165. https://doi.org/10.1144/SP381.15.
Whitehead, J.M., Harwood, D.M., McMinn, A., 2003. Ice-distal Upper Miocene marine strata from inland Antarctica. Sedimentology 50, 531–552. https://doi.org/10.1046/j.1365-3091.2003.00563.x.
Wilch, T.I., Lux, D.R., Denton, G.H., McIntosh, W.C., 1993. Minimal Pliocene-Pleistocene uplift of the dry valleys sector of the Transantarctic Mountains: a key parameter in ice-sheet reconstructions. Geology 21, 841–844. https://doi.org/10.1130/0091-7613(1993)021<0841:MPPUOT>2.3.CO;2.
Wilson, D.S., Luyendyk, B.P., 2006. Bedrock platforms within the Ross Embayment, West Antarctica: Hypotheses for ice sheet history, wave erosion, Cenozoic extension, and thermal subsidence. Geochem. Geophys. Geosyst. 7, 1–23. https://doi.org/10.1029/2006GC001294.
Wilson, D.S., Luyendyk, B.P., 2009. West Antarctic paleotopography estimated at the Eocene-Oligocene climate transition. Geophys. Res. Lett. 36, L16302. https://doi.org/10.1029/2009GL039297.
Wilson, D.S., Jamieson, S.S.R., Barrett, P.J., Leitchenkov, G., Gohl, K., Larter, R.D., 2012. Antarctic topography at the Eocene-Oligocene boundary. Palaeogeogr. Palaeoclimatol. Palaeoecol. 335–336, 24–34. https://doi.org/10.1016/j.palaeo.2011.05.028.
Wilson, D.S., Pollard, D., DeConto, R.M., Jamieson, S.S.R., Luyendyk, B.P., 2013. Initiation of the West Antarctic Ice Sheet and estimates of total Antarctic ice volume in the earliest Oligocene. Geophys. Res. Lett. 40, 4305–4309. https://doi.org/10.1002/grl.50797.